biophysica

MDPI

Article

Quantum Well Model for Charge Transfer in Aperiodic DNA and Superlattice Sequences

Alan Tai [1,2]

[1] College of Natural Sciences, Grand Canyon University, Phoenix, AZ 85017, USA; alan.tai@my.gcu.edu
[2] Department of Physics, Boston College, Boston, MA 02167, USA

Abstract: This study presents a quantum well model using the transfer matrix technique to analyze the charge transfer characteristics of nanostructure sequences in both DNA and superlattices. The unconfined state, or unbound state, above the quantum well is used to investigate carrier behaviors in a semiconductor nanostructure. These analytical approaches can be extended to enhance the understanding of charge transfer in DNA nanostructures with periodic and aperiodic sequences. Experimental validation was conducted through photoreflectance spectroscopy on nanostructures within the semiconductor superlattices. Furthermore, the study's findings were compared with earlier research by Li et al. on the thermoelectric effect and its dependence on molecular length and sequences in single DNA molecules. The results showed agreement, offering novel insights into charge transfer and transport in DNA nanostructures across various sequence types.

Keywords: asymmetry; symmetry; aperiodic sequences; periodic sequences; quasiperiodic; DNA; quantum mechanics; quantum well; charge transfer; nanostructure; Fibonacci; Thue–Morse; superlattices

Citation: Tai, A. Quantum Well Model for Charge Transfer in Aperiodic DNA and Superlattice Sequences. *Biophysica* **2024**, *4*, 411–441. https://doi.org/10.3390/biophysica4030027

Academic Editor: Ivo Crnolatac

Received: 27 June 2024
Revised: 25 August 2024
Accepted: 26 August 2024
Published: 28 August 2024

1. Introduction

DNA plays a crucial role in the development of life on Earth because it holds the library of information that is critical for the "software" operation within all living organisms. Charge transfer [1–4] within DNA enables efficient information assessments and communication necessary for normal cellular function. Analogous to a faster CPU and higher data transfer rate within a computer, the functionality of DNA can be enhanced by increasing the signal speed transmitted along the DNA sequence. Researchers worldwide have extensively investigated the biochemical mechanisms, charge transfer processes, and semiconducting characteristics within DNA [5,6]. Classical mechanical analysis can be extended to quantum mechanical analysis as the dimensions of DNA and semiconductor nanostructures are on a microscopic scale, where quantum modeling can be used. Continued research on DNA through quantum mechanical theory and experiments can enhance our understanding of DNA [7–13].

DNA's structure, initially viewed as periodic, was reinterpreted by Schrödinger as an aperiodic crystal, showing the relationship between symmetry, asymmetry, and information [14]. DNA's biological computations are much more efficient than supercomputers, with supercomputers being about eight orders of magnitude less efficient than the Landauer bound and six orders of magnitude less efficient than biological translation [15,16]. Symmetry and order, both periodic and aperiodic, enhance biological computation efficiency, as single computations act on multiple spots in biological patterns. The informational model of biology is closely related to the Landauer principle, bridging the theory of information to physics and suggesting the thermodynamic equivalent of information, showing the lower theoretical limit of energy consumption of physical and biological computation [15]. Understanding the impact of the periodic and aperiodic sequences of DNA on life requires fundamental studies in mathematical and physical analysis of the basic constituents of nature [16,17]. Two major factors influencing the signaling rate and charge transfer within

DNA sequences relate to quantum tunneling in the short range of the under-barrier effect and hopping in the extensive range of the above-barrier effect. Research has focused on the tunneling region, where electrons or holes transport through molecules via coherent tunneling. Li et al. [1] studied the hopping region in double-stranded DNA, where electrons or holes hop along a molecule sequentially. Their study reveals that DNA thermoelectricity can be tuned by its sequences and length, offering insights for applications in programmable DNA nanostructures and two- and three-dimensional superlattices [18–20].

The hopping mechanism of charge transfer is related to the unconfined energy states or unbound states [21]—those lying above the conduction band barriers or below the valence band barriers—which significantly influence carrier capture and optical transitions [22,23]. The quantum effect extends even into the region above the barriers. The unconfined energy state exhibits continuum characteristics in the quantum well system, unlike the discrete levels of bound states in the confined energy region inside the quantum well.

DNA charge transport (CT), where charges efficiently travel through the interior of the DNA double helix, can conduct charge longitudinally through the π-stacked base pairs. Its unique features extend into various scientific disciplines, including quantum chemistry, quantum physics, and its significance in molecular research and genomic communication. Nanostructured DNA sequences often involve interactions between DNA molecules, metallic nanoparticles, quantum dots, or other nanomaterials. Charge transfer dynamics in these systems are governed by principles of quantum mechanics, molecular physics, and electrochemistry. The fundamental studies aim to reveal the mechanisms and rates of charge transfer processes, including electron and electron hole transfer, across DNA sequences and between DNA and other nanostructured materials. Electronic properties that enable charge transport along the π-stacking interactions facilitate the delocalization of π-electrons, allowing for efficient charge transport over long molecular distances. Therefore, the studies investigate how the sequence, length, conformation, and environment of DNA affect charge transport dynamics. Understanding DNA-mediated charge transport is essential for DNA-based electronic devices, sensors, and nanoelectronics. In general, charge transfer is used when a carrier, created (e.g., by oxidation or reduction) or injected at a specific location, moves to a more favorable location without the application of external voltage. A similar term, "charge transport", is used when the system is held between electrodes and a voltage is applied between these electrodes [24]. DNA is especially sensitive to disruptions, such as environmental change and DNA damage, that alter the dynamics of base pair stacking [25]. To understand the effect of DNA sequencing, environmental factors are usually kept under control in ideal cases (temperature < 295 K) for comparison studies.

The relationship between charge transfer, semiconductors, and computing spans several scientific disciplines, including quantum chemistry, physics, and molecular biology. At its core, charge transfer (CT) involves the movement of charges, such as electrons or electron holes, through a medium of materials, a process central to semiconductor technology and DNA-based nanostructures. The charge transfer dynamics are governed by the principles of quantum mechanics and electrochemistry. The improvement of the carrier's mobility has profound implications for nanotechnology and nanostructures, where the charge transfer in DNA can be applied to develop DNA-based electronic devices, sensors, and components for nanoelectronics [19]. By integrating DNA with other nanostructured materials, such as metallic nanoparticles or quantum dots, scientists can create hybrid systems for three-dimensional DNA-programmable nanoparticle superlattices [26].

In this work, I studied the charge transfer in periodic, Fibonacci, and Thue–Morse DNA sequences by applying transfer matrix techniques to the quantum well model. This quantum well model was validated by comparing the results published in the study on thermoelectric effects and its dependence on molecular length and sequence in single DNA molecules [1].

This paper is organized as follows. The Kronig-Penney model, the transfer matrix method of the quantum wells, and the thermoelectric effect (Seebeck coefficient) in DNA sequences are presented in Section 2. DNA with periodic sequences is simulated to com-

pare with the charge transfer characteristics of aperiodic sequences in Sections 3.1–3.3. The validation of the model by comparing the published results of the thermoelectric effect in DNA sequences is presented in Section 3.4. Bloch wave vector and photoreflectance measurements on different quantum well superlattices (Appendix A) are presented in Section 3.5 to experimentally validate the quantum well model in semiconductor superlattice sequences. The discussion and proposal of future works in both computer simulations and experimental measurements for charge transfer and transport in DNA are presented in Section 4. The conclusion of this study is presented in Section 5. The final session in Appendix A reviews some of the earlier work on the experimental techniques of photoreflectance spectroscopy used to investigate optical transitions between the unconfined states in different superlattice systems.

2. Materials and Methods

2.1. Quantum Wells Modelling of DNA

Kronig and Penney used a one-dimensional square well with periodic potential to calculate the energy band of a general periodic bulk crystal. The same principle can be applied to the quantum well system with periodic sequences and extended to the non-periodic sequence using the effective mass approximation and the transfer matrix technique. The transfer matrix technique takes advantage of the convenience of applying computer methods to solve matrices numerically. The transmission coefficient can then be found to determine the unconfined electron subband energies in the above-barrier region and the confined electron subband energies within the quantum wells.

Referring to Figure 1, the positions of the barriers and wells are located at x_m and x_n respectively, on the x-axis, where the series 1, 2, 3, 4 . . ., m, n. . . are integers in ascending order. The effective mass m* in region M(well) and region N(barrier) are m_w and m_b respectively, where the series 1, 2, 3, 4 . . .M, N. . . are integers in ascending order.

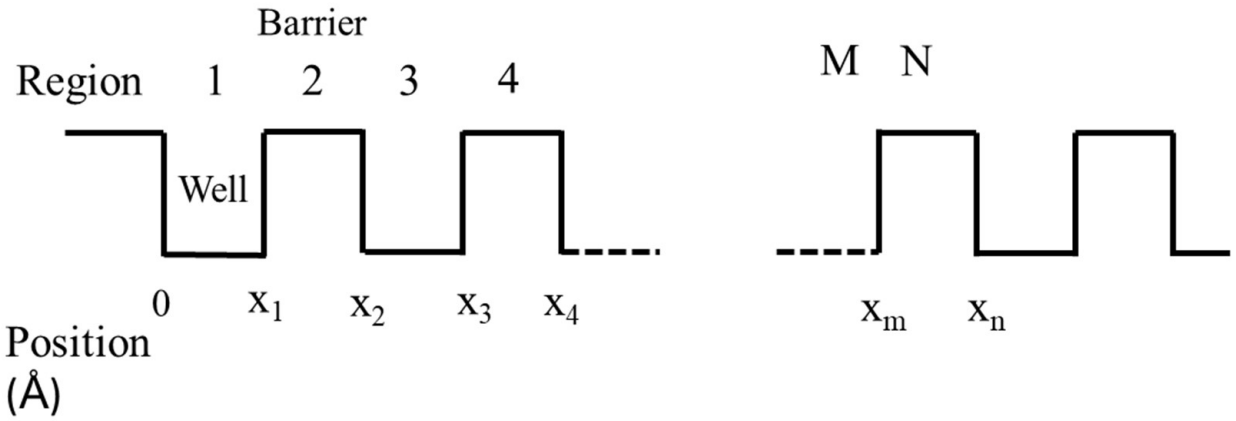

Figure 1. The DNA nanostructure sequence along the x-axis, where the index m, n; M, N are any integer number.

The solutions of the Schrodinger equations in the various regions are:

$$\text{(well)} \quad \psi_M(x) = A_m e^{ikx} + B_m e^{-ikx} \text{ for } x_{m-1} < x < x_m \tag{1}$$

where $k = \left(\frac{2m* E}{h^2}\right)^{1/2}$ corresponds to the wave number in the well region.

$$\text{(barrier)} \quad \psi_{M+1}(x) = A_{m+1} e^{iqx} + B_{m+1} e^{-iqx} \text{ for } x_m < x < x_{m+1} \tag{2}$$

where $q = \left(\frac{2m* (E-V)}{h^2}\right)^{1/2}$ corresponds to the wave number in the barrier region.

E is the energy above the bottom of the well and V is the potential at the top of the barrier. By employing the boundary conditions for the continuity of the wavefunctions and their derivatives, we can form a sequence of 2 × 2 transfer matrices.

The transfer matrix corresponding to the boundary located at x_m is:

$$T(x_m) = \begin{pmatrix} \left(\frac{q+k}{2k}\right)e^{i(q-k)x_m} & -\left(\frac{q-k}{2k}\right)e^{-i(q+k)x_m} \\ -\left(\frac{q-k}{2k}\right)e^{i(q+k)x_m} & \left(\frac{q+k}{2k}\right)e^{-i(q-k)x_m} \end{pmatrix} \quad (3)$$

The transfer matrix corresponding to the boundary located at x_{m+1} is:

$$T(x_{m+1}) = \begin{pmatrix} \left(\frac{q+k}{2q}\right)e^{-i(q-k)x_{m+1}} & \left(\frac{q-k}{2q}\right)e^{-i(q+k)x_{m+1}} \\ \left(\frac{q-k}{2q}\right)e^{i(q+k)x_{m+1}} & \left(\frac{q+k}{2q}\right)e^{i(q-k)x_{m+1}} \end{pmatrix} \quad (4)$$

The final transfer matrix is given by the product,

$$\overleftrightarrow{T} = \prod_i T_i \qquad i = 1, 2, 3 \ldots m, m+1, \ldots \quad (5)$$

and the corresponding transmission coefficient, t = $1/T_{11}$, where T_{11} is the final diagonal component of the matrix $\overleftrightarrow{T}$.

2.2. Simulation of DNA Sequences

Using the above theoretical model, three different sequences were simulated based on the four types of nucleotides found in DNA: adenine (A), thymine (T), guanine (G), and cytosine (C) for the unconfined states in the above-barrier region using the transfer matrix techniques described in Section 2.1. First, periodic sequenced DNA was simulated, and then two aperiodic sequences, or quasiperiodic DNA sequences, namely the Fibonacci sequence and the Thue–Morse sequence were simulated.

To show relationships between the charge transfer of DNA and the simulation model, I used a one-dimensional sequence with 1 or 0 to simulate the sequence of quantum wells and barriers, respectively, for the corresponding nucleotides. The DNA sequences under study are composed of repeated stacks of nucleobases formed by either G-C/C-G as the well (1) or A-T/T-A as the barrier (0). The energy levels between G-C and A-T base pairs are shifted by about 0.4 eV [27]. This difference in energy levels forms the quantum wells and barriers, as shown in Figure 2. Both base pairs have the same nucleotide length of 3.4 Å for each basic unit of 0 or 1 and are counted as 1 layer in the simulation parameters. The helical chains of nucleotides in DNA are bound to each other by hydrogen bonds that coil into tight loops to form different shapes of polymers. Conductivity has been found to be dependent on sequence, hydration, length, temperature, and hybridization in some experiments. Environmental and helical factors are not considered and are assumed to be constant among different DNA sequences for comparison under this basic 1-D model. Table 1 shows the effective masses of electrons and holes along directions perpendicular to the stacking planes (in units of the free electron mass m_0) [28]. The effective mass of electrons m_e of 5 is used for the simulation of charge transfer based on the average of G-C combinations in Table 1. Note that the m_e and m_h (effective mass of holes) have the same order of magnitude for the DNA nucleotides. The m_e is an empirical value determined by experiments and the calculated lattice parameters. This value can be adjusted for changes in environmental factors to match the simulation results and experiments, as discussed in future work in Section 5.

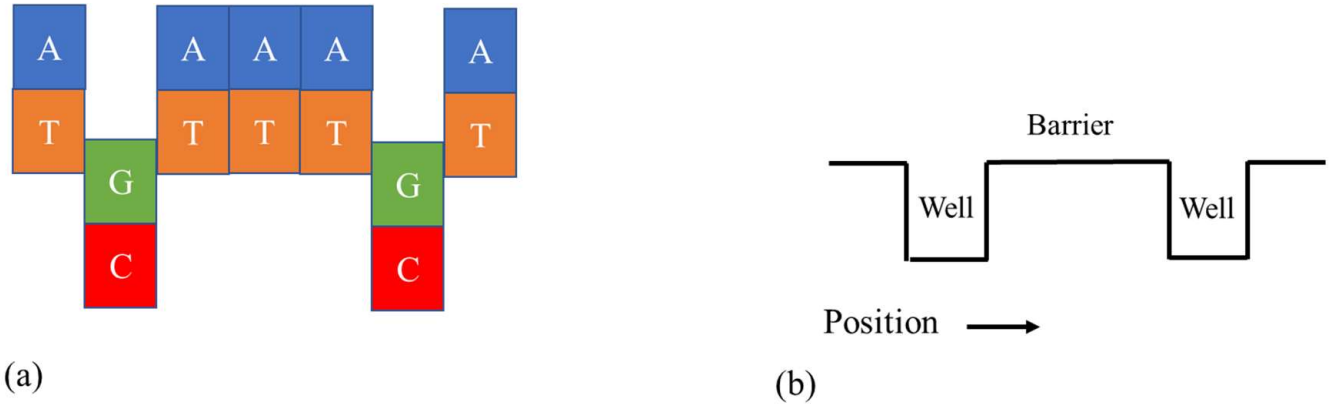

Figure 2. Schematic representation of the energy profile in DNA with 7 base pairs. (**a**) Ionization potential for G-C base pairs differs from A-T base pairs by about 0.4 eV. (**b**) System (**a**) can be treated as a series of quantum wells and barriers systems in different positions.

Table 1. Anhydrous crystals of DNA nucleobases with effective masses of electrons and holes along directions perpendicular to the stacking planes (in units of the free electron mass m_0) are shown [28].

DNA Nucleobases	m_e	m_h
G	4.0	4.0
A	5.4	3.8
C	5.8	3.5
T	6.3	15

2.3. Seebeck Coefficient and Transmission Coefficient

The Seebeck effect is a thermoelectric phenomenon that generates voltage due to temperature differences, caused by the movement of charge carriers. The thermoelectric effect, a fundamental property of materials, is essential for energy conversion, temperature sensing, and regulation. In single molecules, this effect differs significantly from that in bulk materials. Studying the thermoelectric effect in single molecules not only has potential applications but also aids in understanding molecular orbital level alignment and energy conversion mechanisms associated with charge transport. The Seebeck coefficient of a material is a measure of the magnitude of an induced thermoelectric voltage in response to a temperature difference across that material, as induced by the Seebeck effect.

Li et al. [1] explore the thermoelectric effect in double-stranded DNA (dsDNA) molecules. By selecting different DNA sequences, the study examines the thermoelectric effect in both the tunneling regime and the hopping regime. In the hopping regime, electrons or holes move sequentially via multiple steps, resulting in a linear dependence of molecular resistance with length. The findings reveal that DNA thermoelectricity can be adjusted based on its sequences and length, offering new insights into the thermoelectric effect in single molecules and laying the groundwork for potential applications with programmable DNA nanostructures, a rapidly advancing field.

Using their results on the thermoelectric effect in different DNA sequences [1], I compared qualitatively their results with the simulation of the transmission coefficient on the same DNA sequences to validate the model. The Seebeck coefficient is proportional to the slope of the transmission probability $T(E)$ at Fermi energy E_F, where k_B, T, and e are the Boltzmann constant, temperature, and electron charge, respectively [16].

$$S(E_F, T) \approx \frac{\pi^2 (k_B)^2 T}{3e} \left(\frac{\partial \ln(T(E))}{\partial E} \right)_{E=E_F} \quad (6)$$

3. Results

3.1. Periodic DNA

We first simulated the periodic sequence of DNA, with alternating layers of 0 and 1, for the energy states above the quantum well, as shown in Figure 3. The periodic structure is arranged in a repeating fashion like 011011011011011011... 44 boundaries and 172 boundaries are selected to compare with other types of DNA using a similar number of layers. Each layer of nucleotides corresponds to either 1 or 0 according to the periodic sequence. Each barrier (0) or well (11, well width of 3.4 Å × 2 = 6.8 Å) has two boundaries on the left and right sides, as shown in Figure 3. We used the analytical approach described in Section 2 to formulate this simulation.

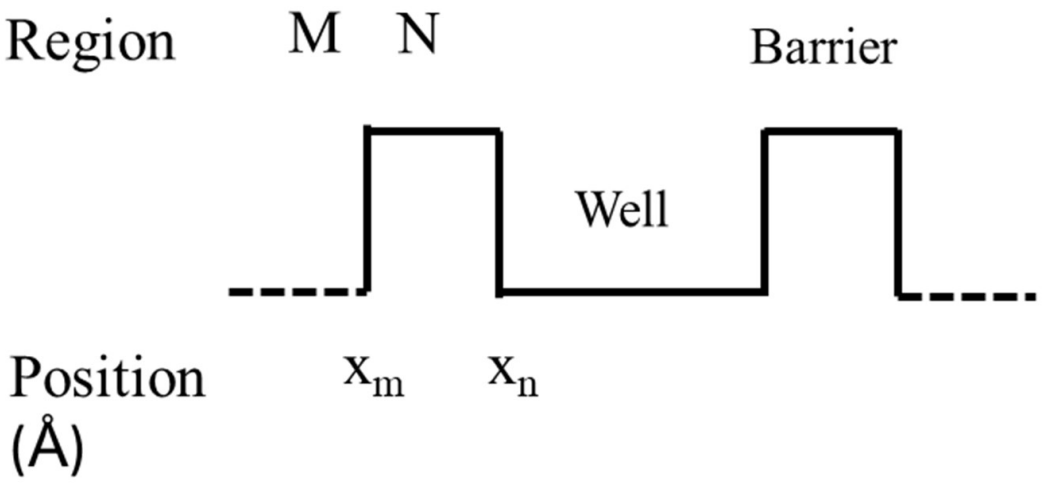

Figure 3. The periodic DNA nanostructure sequence with repeated 011011011... along the x-axis to form different boundaries of DNA, where the index m, n; M, N are any integer number.

The simulation results in Figure 4a,b show the transmission coefficient vs. energy level for 44 boundaries and 172 boundaries, respectively, in meV above the bottom of the quantum well in the conduction band structure of a DNA sequence. Our focus is on the region above the barrier height of 400 meV, where there is a gap from 400 meV to 515 meV, followed by a band up to 764.1 meV. Subsequent gaps and bands appear after the first band, depending on how far into the continuum of the unconfined region the simulation extends. The number of peaks oscillating in the band increases with the number of boundaries, rising from 44 boundaries to 172 boundaries, as calculated by the computer simulation. However, the corresponding positions of gaps and bands remain the same when compared between the two simulation results in Figure 4a,b.

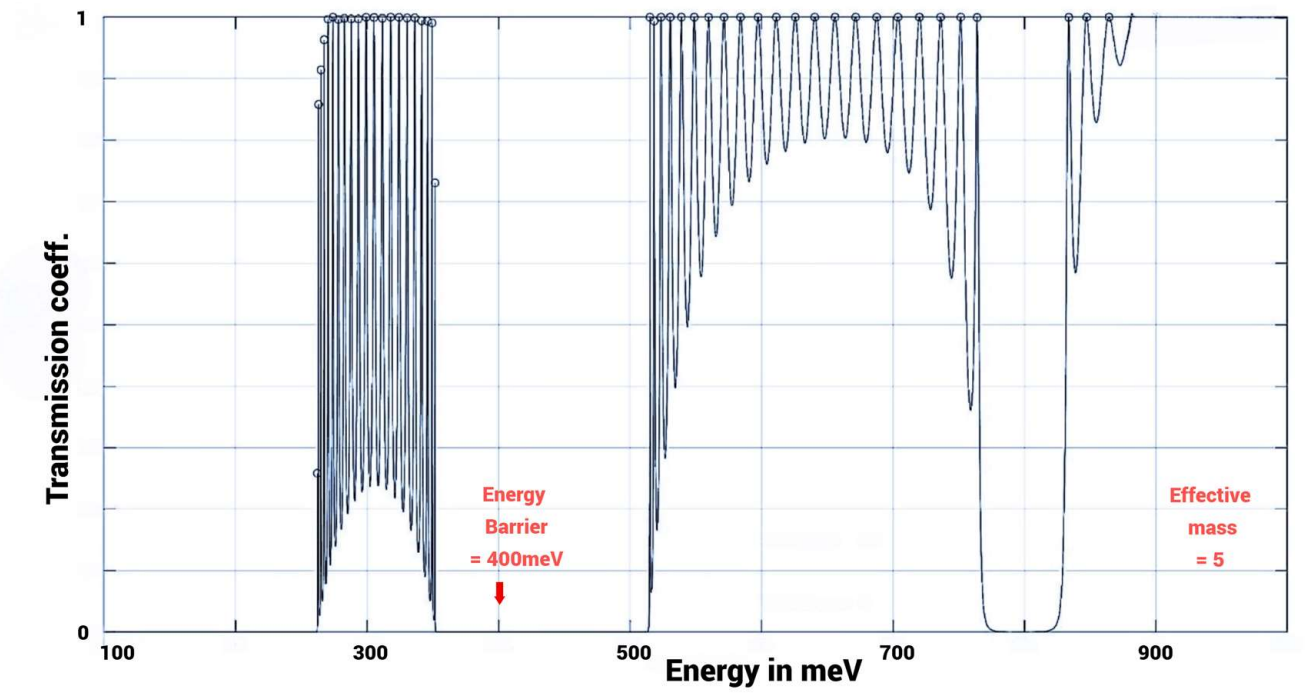

(**a**)

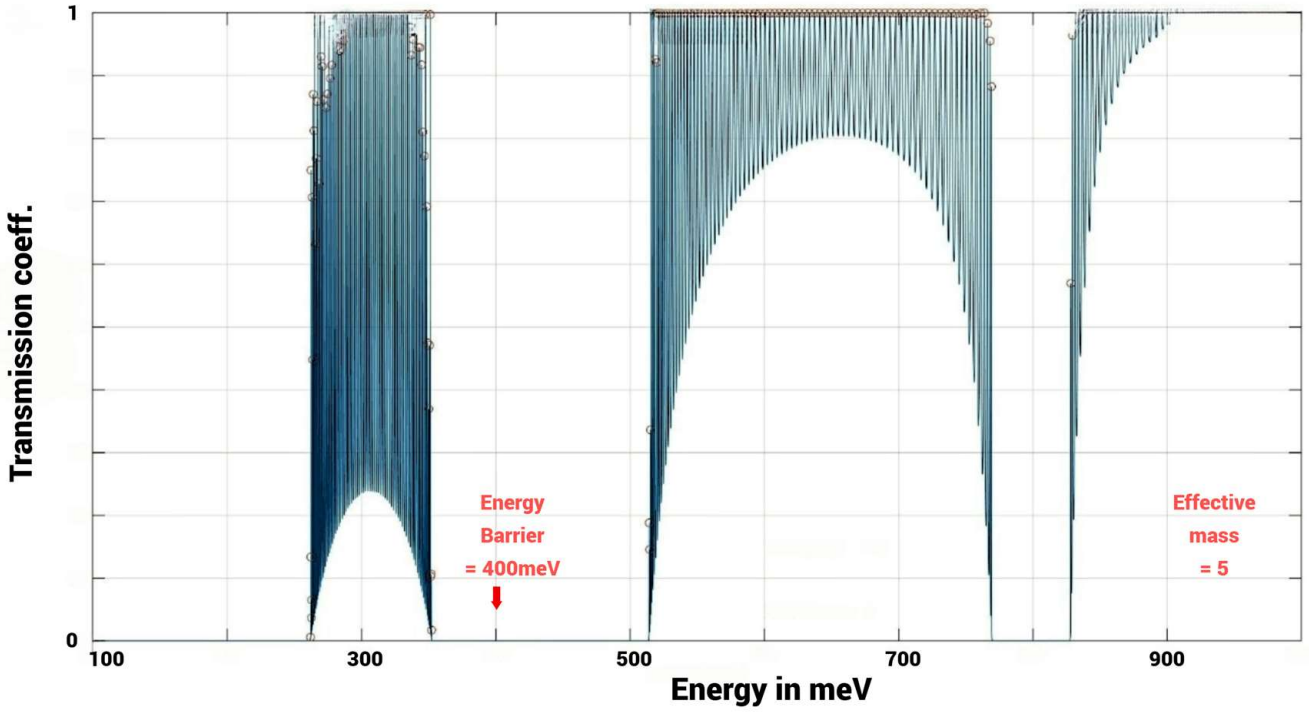

(**b**)

Figure 4. Computer simulation of transmission coeff. vs. energy for periodic DNA, quantum barrier = 400 meV, and electron effective mass me = 5 with (**a**) 44 boundaries and (**b**) 172 boundaries. (The circles correspond to the peaks of the graph).

3.2. Fibonacci Sequenced DNA

A quasiperiodic sequence of DNA, with layers arranged according to the Fibonacci sequence, is shown in Table 2.

Table 2. Fibonacci sequenced DNA in 0 and 1 sequence.

layer 1–32	01011010110110101101011010110
layer 33–64	11010110101101101011010110110101
layer 65–96	10110101101011011010110110101101
layer 97–128	01101101011010110110101101101011
layer 129–160	01011011010110101101101011011010
layer 161–192	11010110110101101101011010110110
layer 193–224	10110101101101011011010110101101
layer 225–256	10101101101011010110110101101011

Note that in the sequence limit, the ratio of the (majority 1) basis over the (minority 0) basis will approach the golden mean value or golden ratio $\tau = (1 + \text{sqrt}(5))/2 \sim 1.618$.

The Fibonacci sequence formula for "Fn" is defined using the recursive formula setting F0 = 0, F1 = 1, and using the formula below to find Fn. The Fibonacci formula is given as follows:

$$Fn = F(n - 1) + F(n - 2), \text{ where } n > 1.$$

Fn represents the (n + 1)th number in the sequence, and
F(n – 1) and F(n – 2) represent the two preceding numbers in the sequence.

The Fibonacci sequence formula is used to compute the terms of the sequence to obtain a new term. In this Fibonacci sequenced DNA, the 0 and 1 are grouped together instead of being mathematically added. For example, the first two terms of the Fibonacci sequence are 0 and 1, and the third term is obtained by grouping the above formula as follows:

$$F3 = F1 + F2 = 0 + 1 = 01.$$

$$F4 = F2 + F3 = 101$$

$$F5 = F3 + F4 = 01101$$

$$F6 = F4 + F5 = 10101101$$

$$F7 = F5 + F6 = 0110110101101$$

In the same way, the other terms of the Fibonacci sequence using the above formula can be combined as shown in the sequence below:

layer 1–32 (0)(1)(01)(101)(01101)(10101101)(011011010110

layer 33–64 1)(10101101011010101101)(0110110101. . .

In this Fibonacci sequence of 0 and 1, there are wells with only one layer of "1" and a maximum of two layers of "1" together to form smaller and larger quantum wells, respectively. Each large and small quantum well has two boundaries, but the large quantum well has two layers of nucleotides, while the small quantum well has only one layer of nucleotides. There is only one layer of "0" with two boundaries in between the quantum wells of the Fibonacci sequenced DNA. Additionally, there is a mirror image at layer 28 with layers 1–27 and layers 29–55, corresponding to the 44th boundaries of the quantum well and barrier sequence.

The simulation results in Figure 5a–c show the transmission coefficient vs. energy level for (a) $m_e = 5$ with 44 boundaries, (b) $m_e = 5$ with 100 boundaries, and (c) $m_e = 3.5$ with 44 boundaries, respectively, in meV above the bottom of the quantum well (QW) in the conduction band structure of the Fibonacci sequenced DNA. There are distinct and narrow transmission peaks separated from each other inside the quantum well region (<400 meV) and in the initial band in the unconfined region (>400 meV). When the simula-

tion boundaries increase from (a) 44 to (b) 100 for m_e = 5, the transmission peaks inside the quantum well decrease. However, the transmission peaks, increase in the unconfined region. The corresponding positions of gaps and bands remain the same when comparing the two simulation results in Figure 5a,b. In Figure 5c, m_e = 3.5 with 44 boundaries is used in a simulation to see how the change in m_e affects the transmission peaks. The results of the simulation show that the relative positions of the band and gaps are shifted to the right. Additionally, some transmission peaks appear just above the quantum well in the unconfined region.

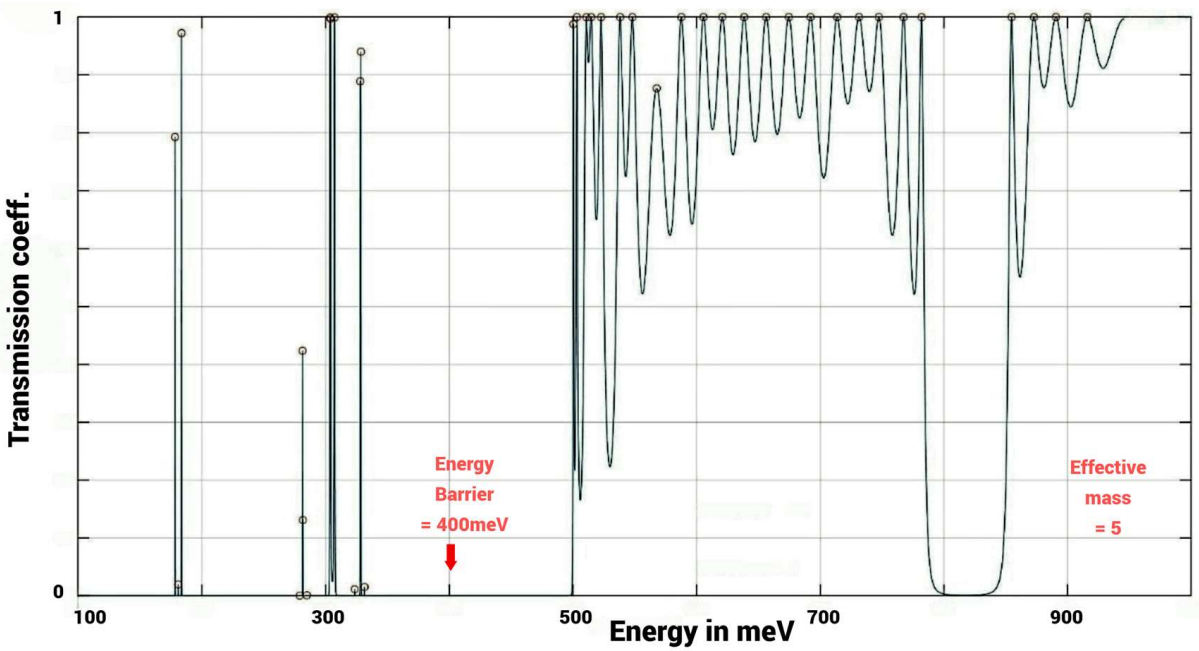

(**a**)

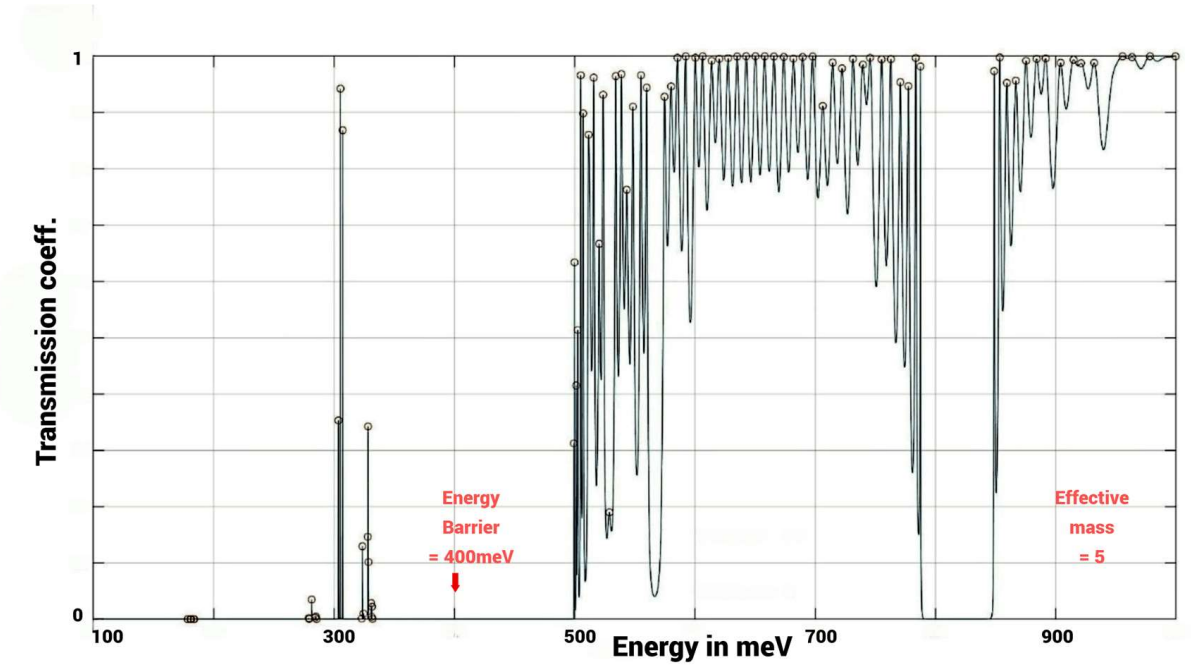

(**b**)

Figure 5. *Cont.*

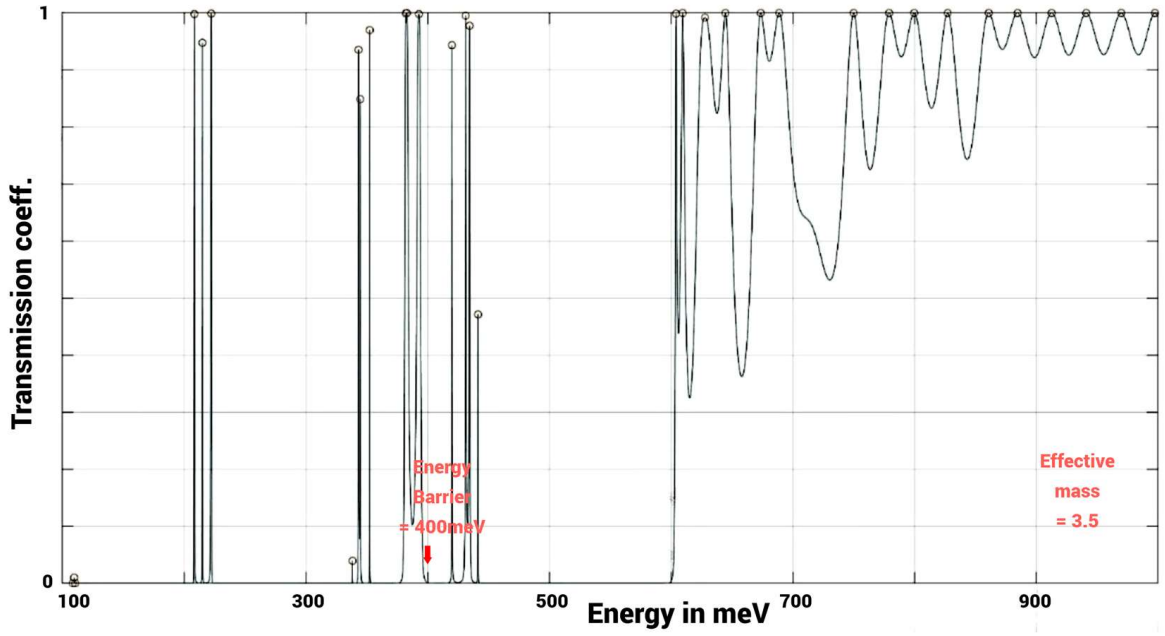

(**c**)

Figure 5. Computer simulation of transmission coeff. vs. energy for Fibonacci sequenced DNA, quantum barrier = 400 meV and (**a**) m_e = 5 with 44 boundaries, (**b**) m_e = 5 with 100 boundaries, (**c**) m_e = 3.5 with 44 boundaries.

3.3. Thue–Morse Sequenced DNA

Thue–Morse [29] DNA, with layers of barriers and wells arranged according to a special sequence called the "Thue–Morse" sequence, is shown in Table 3. The purpose is to form a sequence that is the opposite (barrier becomes well; well becomes barrier) of the entire sequence before it.

Table 3. Thue–Morse sequenced DNA in 0 and 1 sequence.

layer 1–32	01101001100101101001011001101001
layer 33–64	10010110011010010110100110010110
layer 65–96	10010110011010010110100110010110
layer 97–128	01101001100101101001011001101001
layer 129–160	10010110011010010110100110010110
layer 161–192	01101001100101101001011001101001
layer 193–224	01101001100101101001011001101001
layer 225–256	10010110011010010110100110010110

Note that the arrangement of layers 1–64 is the same as layers 193–256; layers 65–128 are the same as layers 129–192.

For example:
The first layer is 0 (barrier), the second layer is 1 (well),
the third and fourth layers will be 10 (well and barrier),
the fifth to eighth layers will be 1001 (well, barrier, barrier, and well).
Therefore, the sequence will be:
0 1 10 1001 and so on.

The simulation results in Figure 6a,b show the transmission coefficient vs. energy level for (a) m_e = 5 with 44 boundaries and (b) m_e = 5 with 172 boundaries, respectively, in meV above the bottom of the QW in the conduction band structure of the Thue–Morse sequenced DNA. There are distinct and narrow transmission peaks separated from each other inside the quantum well region (<400 meV) and in the initial band in the unconfined region (>400 meV). When the simulation boundaries increase from (a) 44 to (b) 172 for $\mathbf{m_e}$ = 5, the transmission peaks inside the quantum well stay in the same position, but

the number of transmission peaks increases (in oscillation) in the unconfined region. The corresponding positions of gaps and bands remain the same when comparing the two simulation results in Figure 6a,b.

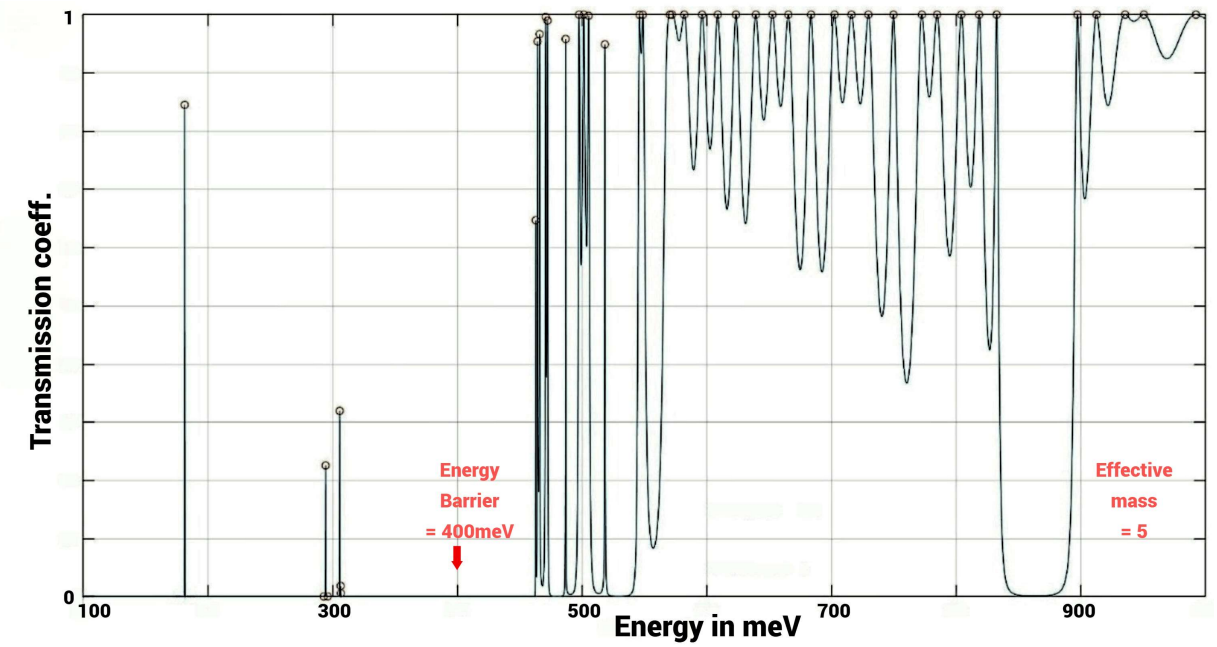

(**a**)

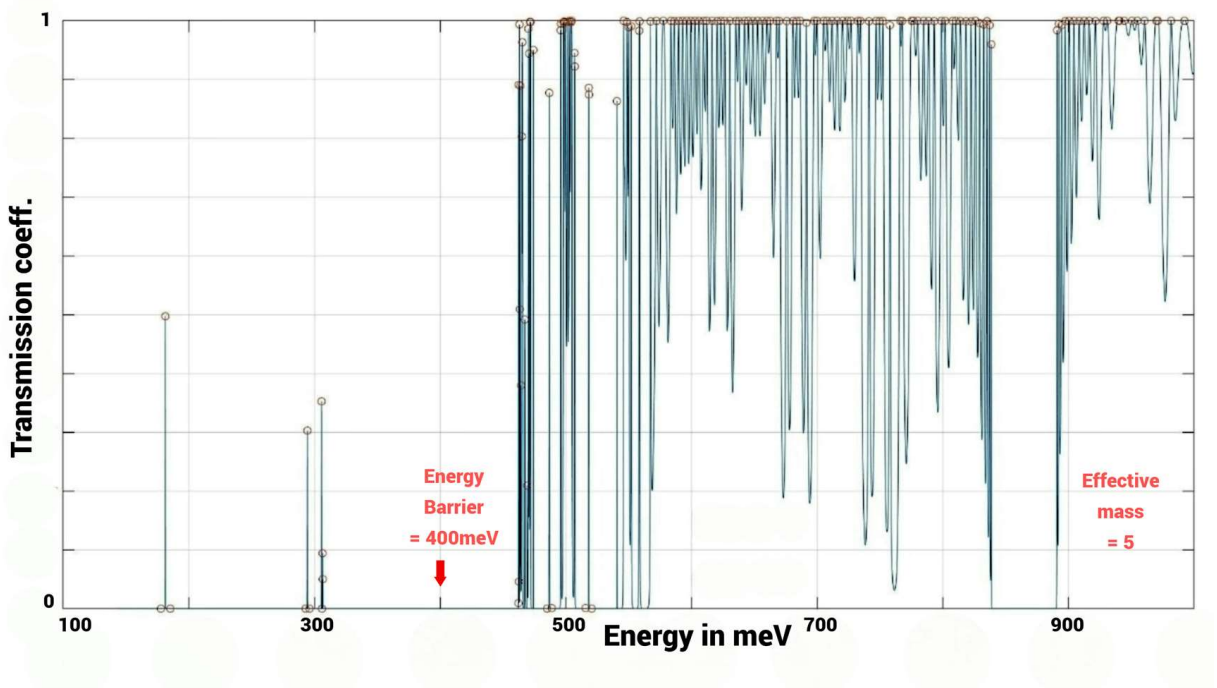

(**b**)

Figure 6. Computer simulation of transmission coeff. vs. energy for Thue–Morse sequenced DNA, quantum barrier = 400 meV and electron effective mass = 5 with (**a**) 44 boundaries and (**b**) 172 boundaries.

3.4. Validation of the Model

The quantum well model is initially used to determine whether the simulation of DNA sequences can exhibit agreement with related experimental results. Although the quantum effect on the nanostructure of superlattices is quite similar to that on the DNA structure, various factors, such as chemical composition and environment, can generate different results in simulation. Therefore, this study focuses on the intrinsic effects on DNA by comparing different DNA sequences, while all other key parameters are treated as constant. All the simulations and experiments are conducted under the same environmental and thermal conditions, with the varying factor being the different DNA sequences.

The results published by Li et al. [1] are utilized to compare the simulations obtained from the quantum well model in this study. The Seebeck coefficients of DNA in the hopping regime (in A(CG)nT) are small and weakly dependent on molecular length compared to other organic molecules. Inserting a short AT block (shorter than 5 AT base pairs) into the middle of A(CG)nT leads to a much greater Seebeck coefficient, which increases with the AT block length. However, when the AT block is longer than 5 AT base pairs, the Seebeck coefficient drops to the level of A(CG)nT and becomes less sensitive to the AT length. This transition coincides with the tunneling-hopping transition near 4–5 AT base pairs observed from a conductance measurement, strongly suggesting that the thermoelectric effect is large in the tunneling region and small in the hopping region.

Figure 7a–d shows the computer simulation of the transmission coefficient vs. energy for different DNA lengths: (a) $A(CG)_3T$, (b) $A(CG)_5T$, (c) $A(CG)_6T$, and (d) $A(CG)_7T$, with a quantum barrier of 400 meV and an electron effective mass of 5. All the plots show distinct peaks in both the quantum well regions (<400 meV) and the unconfined regions (>400 meV). The transmission peaks inside the quantum wells correspond to the tunneling region, based on the theory of quantum mechanics. The transmission peaks outside the quantum wells in the unconfined region correspond to the hopping region. These results qualitatively show that there are combinations of both tunneling and hopping transitions in the DNA sequences.

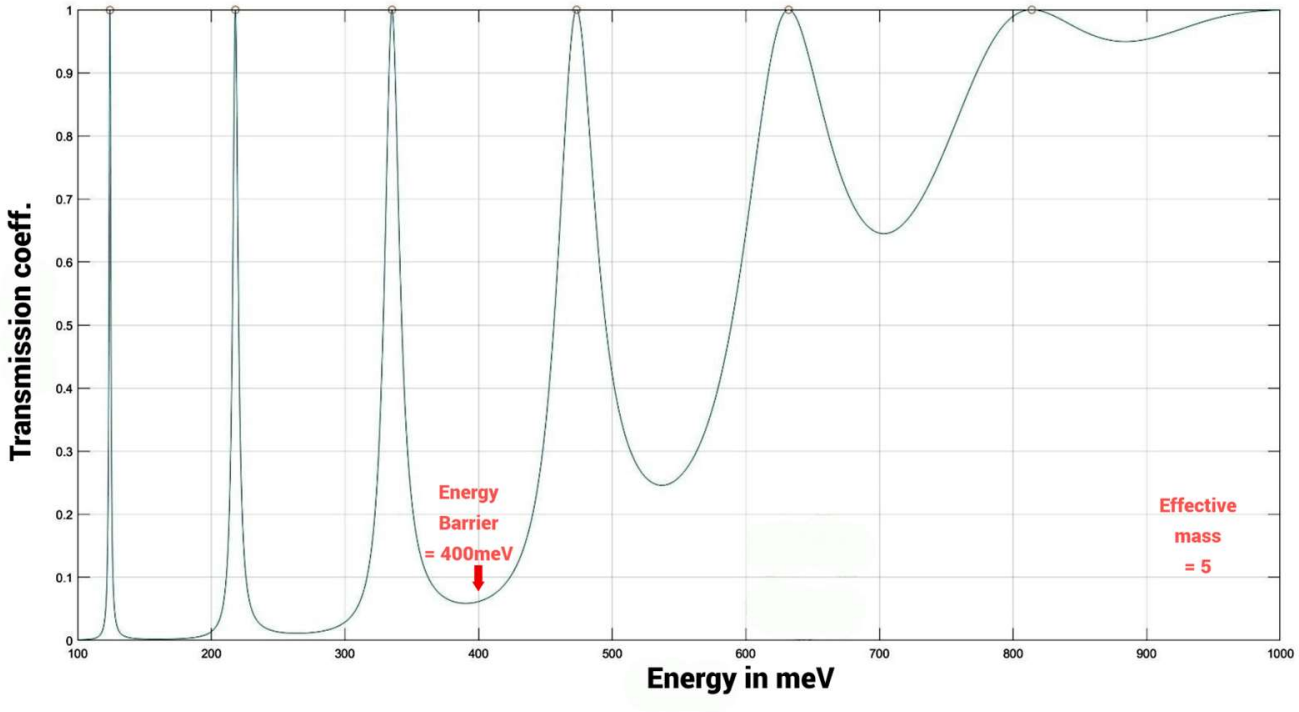

(**a**)

Figure 7. *Cont.*

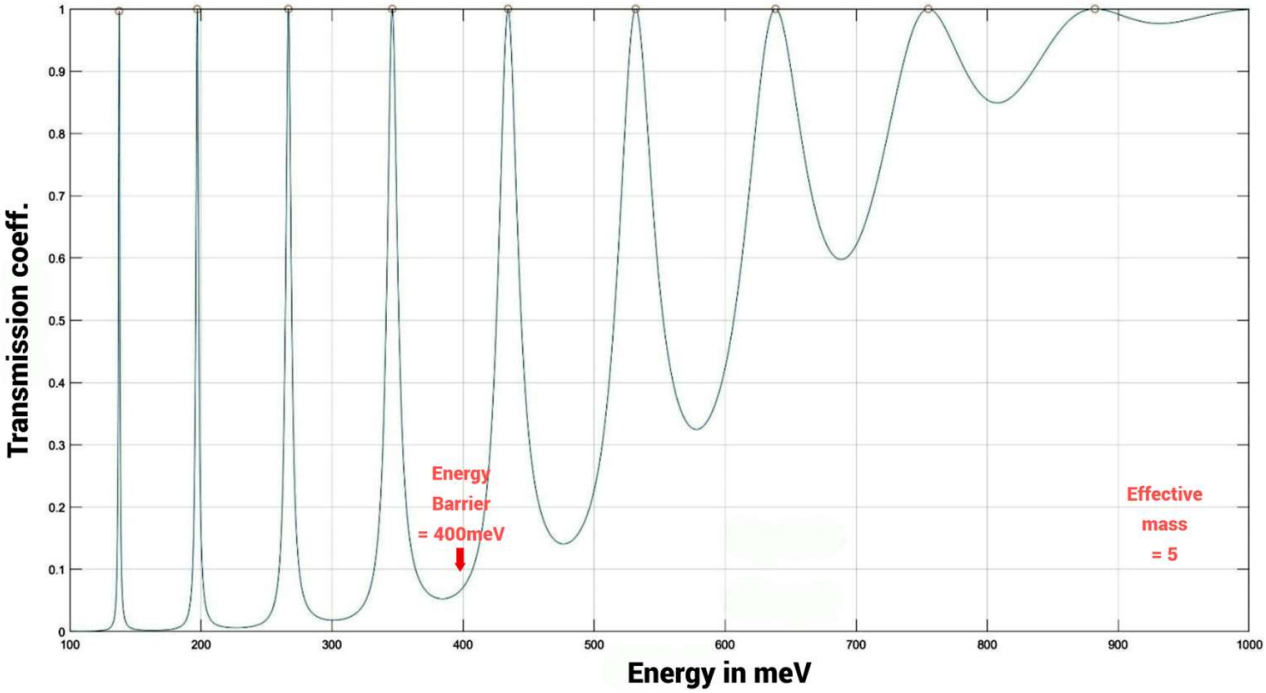

(**b**)

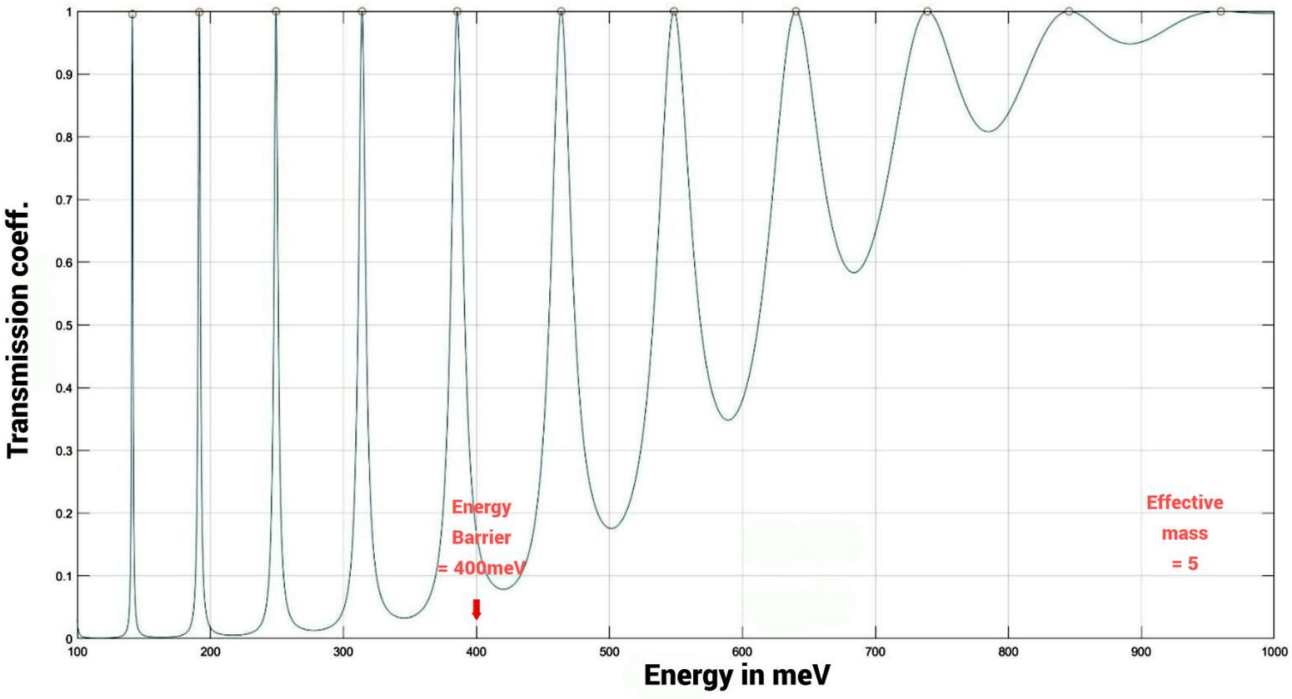

(**c**)

Figure 7. *Cont*.

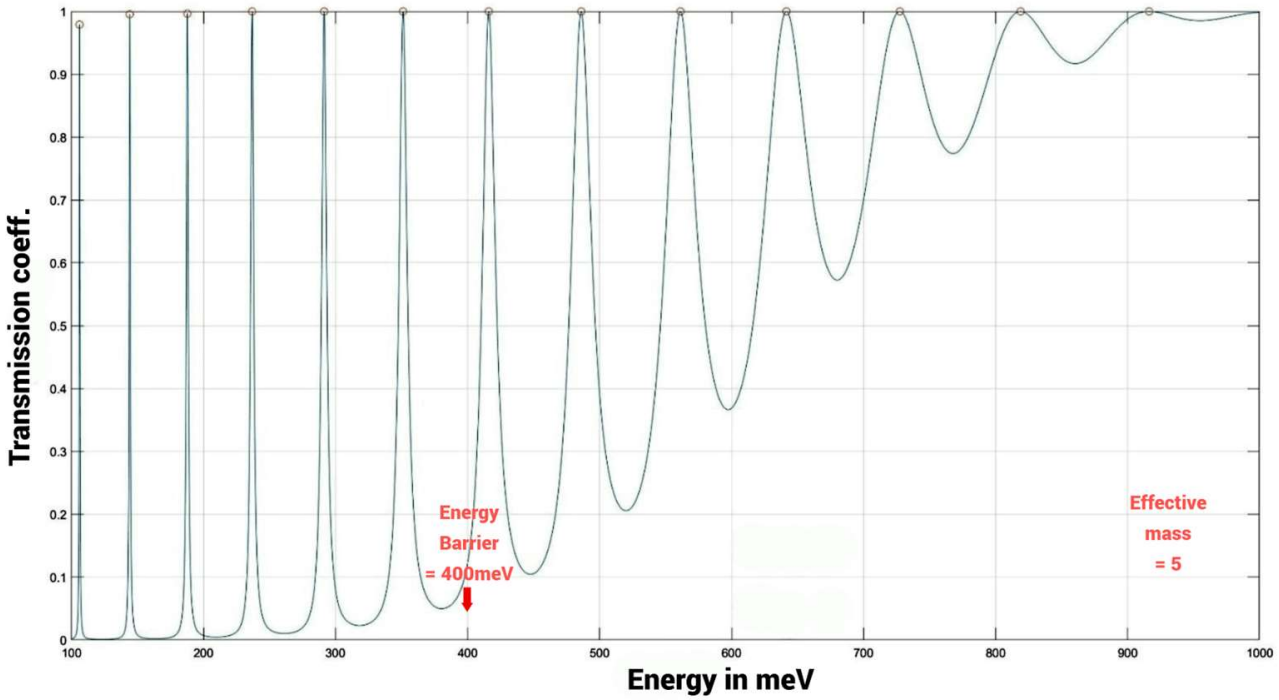

(**d**)

Figure 7. Computer simulation of transmission coeff. vs. energy for different DNA lengths: (**a**) $A(CG)_3T$, (**b**) $A(CG)_5T$, (**c**) $A(CG)_6T$, and (**d**) $A(CG)_7T$; quantum barrier = 400 meV and electron effective mass = 5.

Figure 8a–g shows the computer simulation of transmission coefficient vs. energy for different DNA lengths: (a) ACGCAGCGT, (b) ACGCATGCGT, (c) ACGCATAGCGT, (d) $ACGC(AT)_2GCGT$, (e) $ACGC(AT)_2AGCGT$, (f) $ACGC(AT)_3GCGT$, and (g) $ACGC(AT)_4GCGT$, with a quantum barrier of 400 meV and an electron effective mass of 5. By inserting a short AT block (a–d, shorter than 5 AT base pairs) into the middle of A(CG)nT, the transmission peaks inside the quantum wells (E < 400 meV) progressively reduce to a smaller peak in Figure 8d (4 AT base pairs). With 5, 6, and 8 AT base pairs, the transmission peaks inside the quantum wells (E < 400 meV) gradually disappear (t < 0.08), but the unconfined region (E > 400 meV) retains some well-defined transmission peaks (t = 1), as shown in Figure 8e–g.

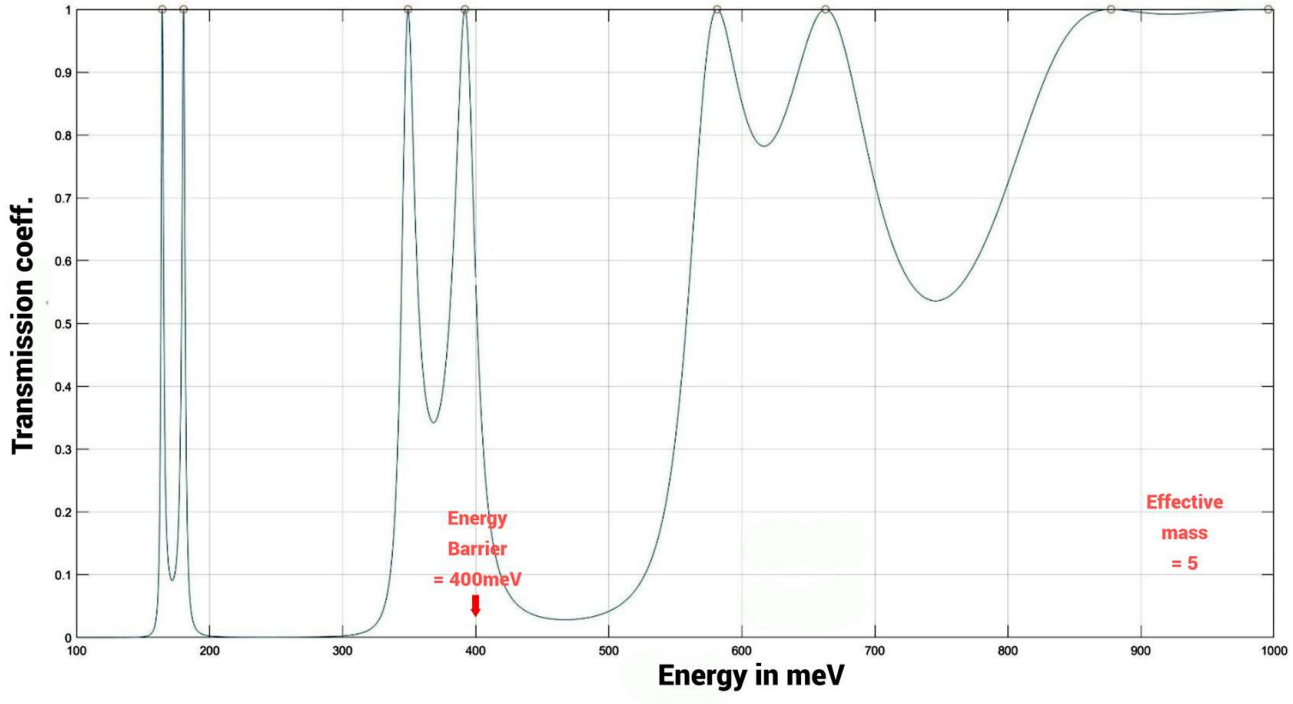

(**a**)

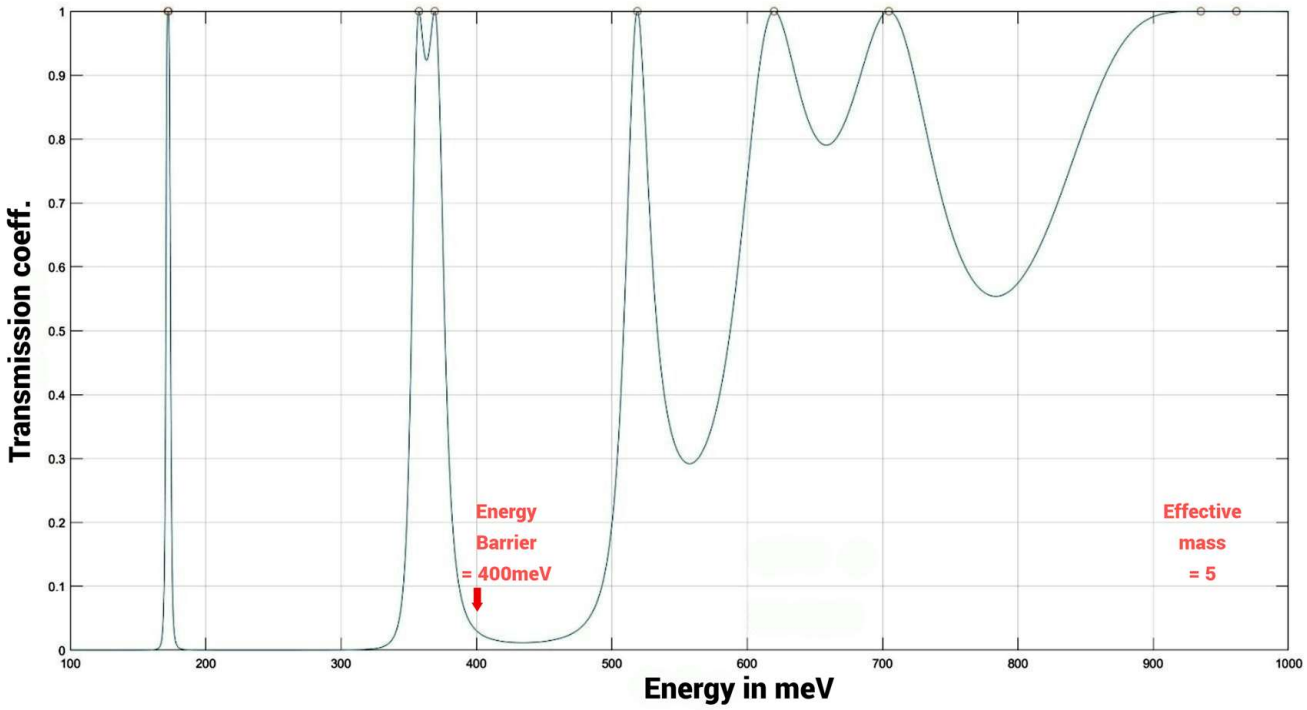

(**b**)

Figure 8. *Cont.*

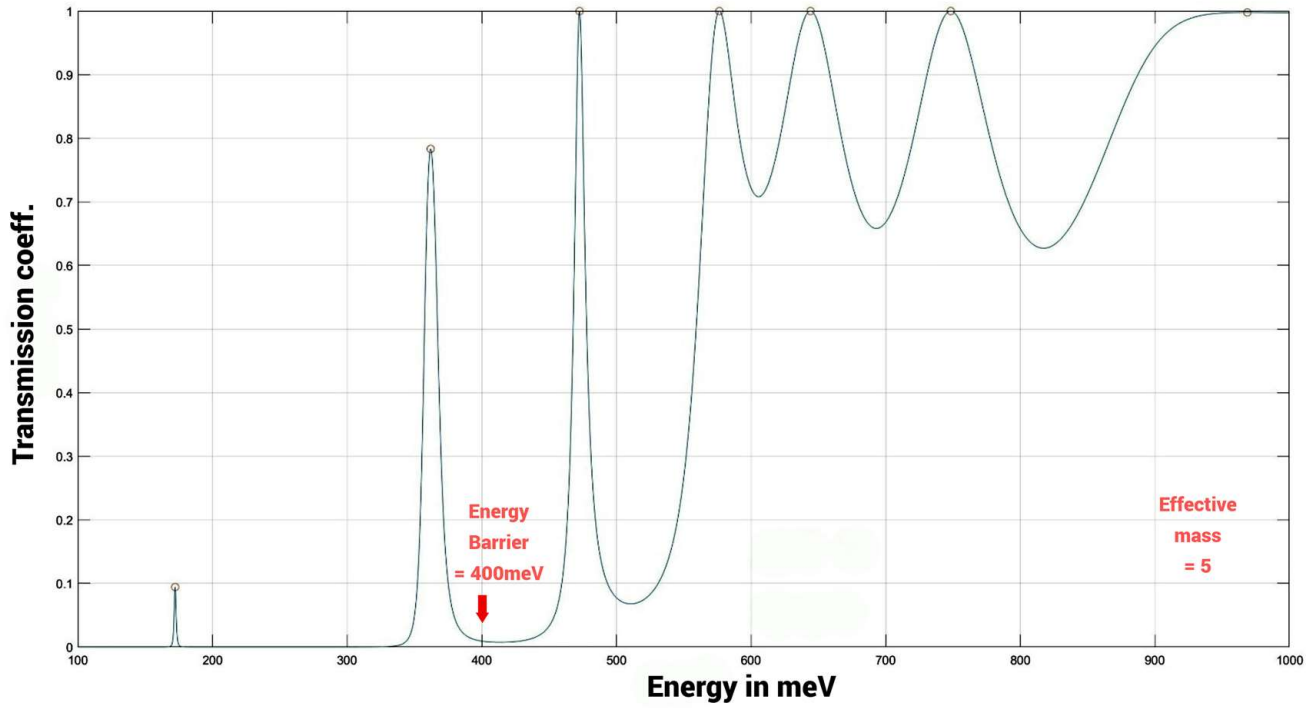

(**c**)

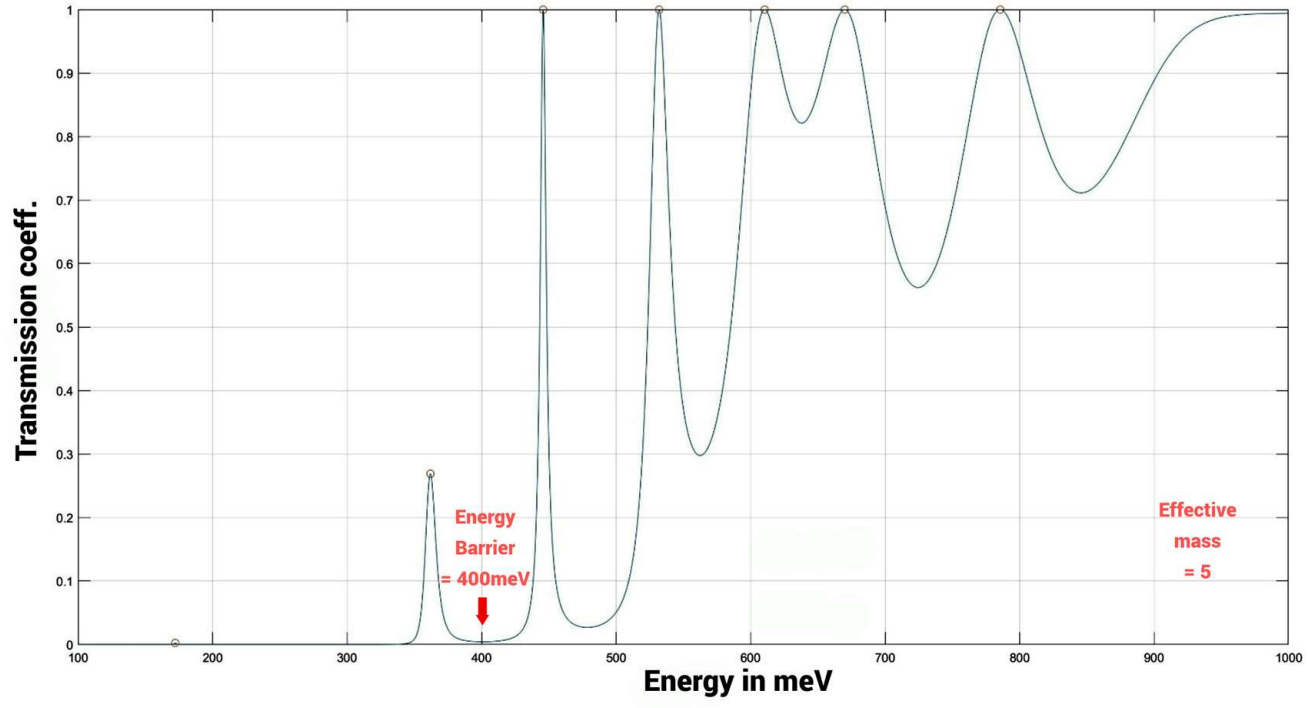

(**d**)

Figure 8. *Cont.*

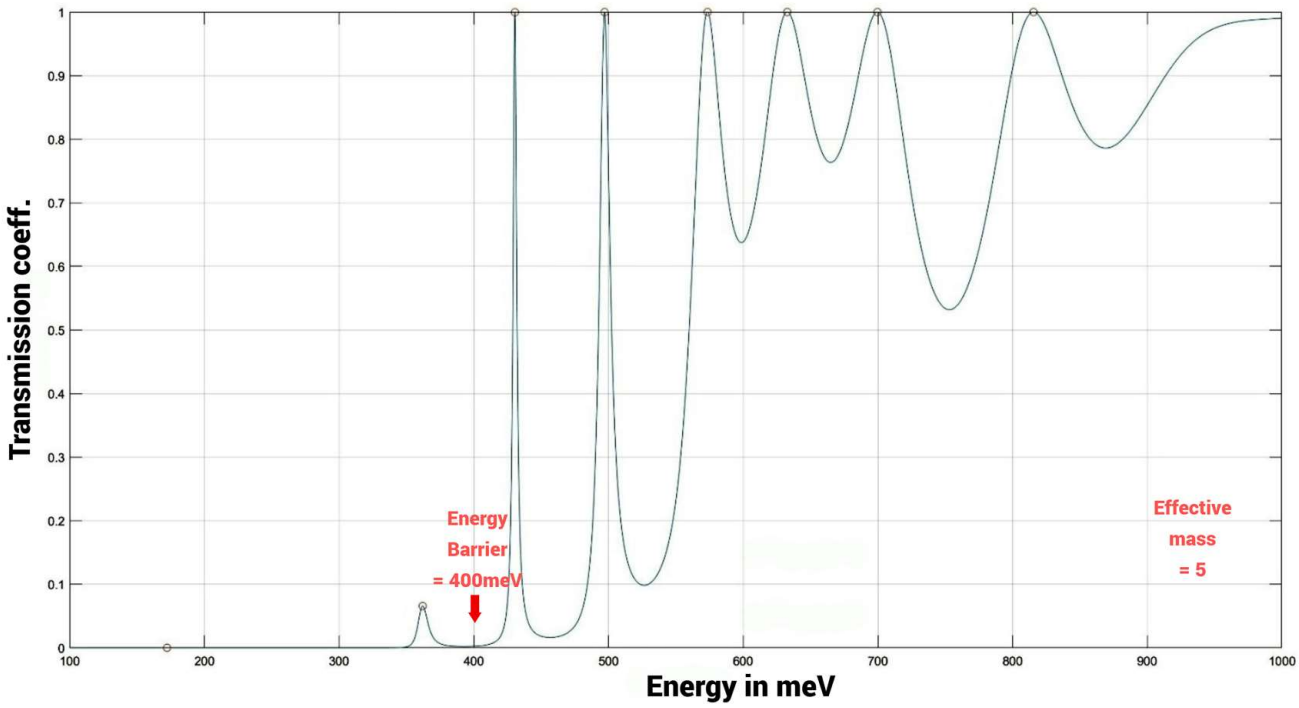

(**e**)

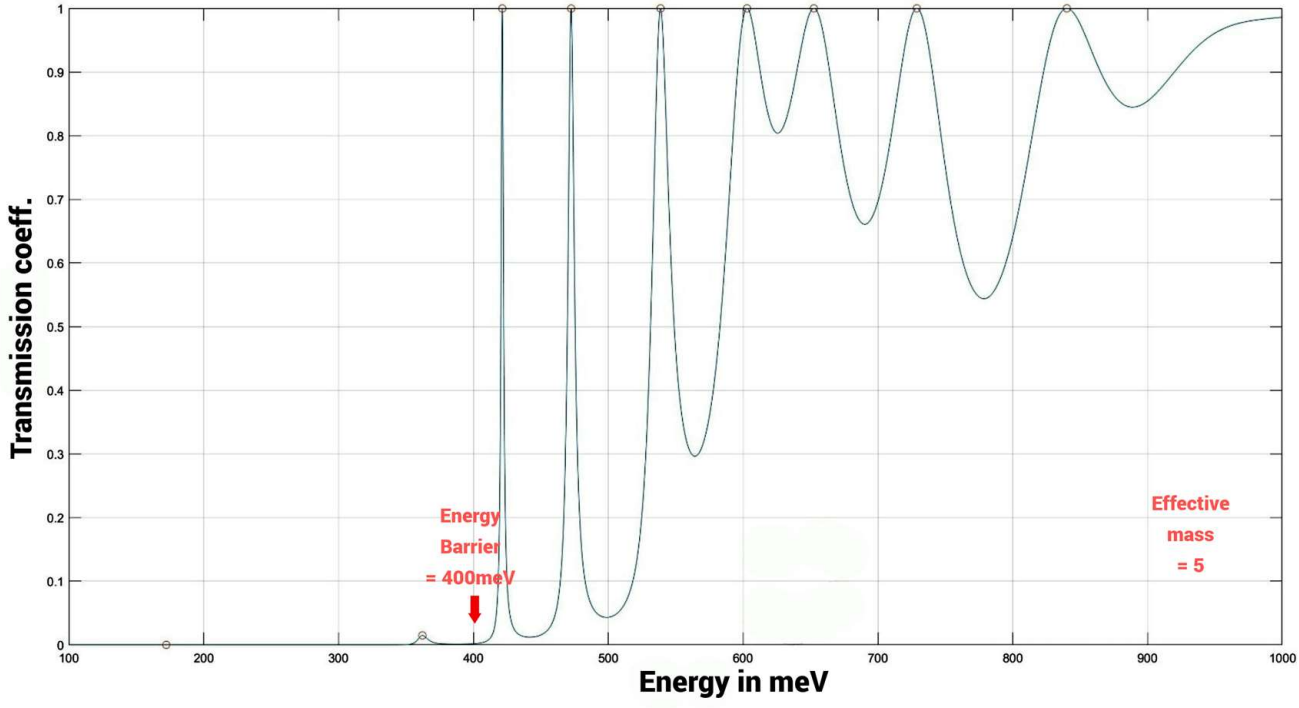

(**f**)

Figure 8. *Cont.*

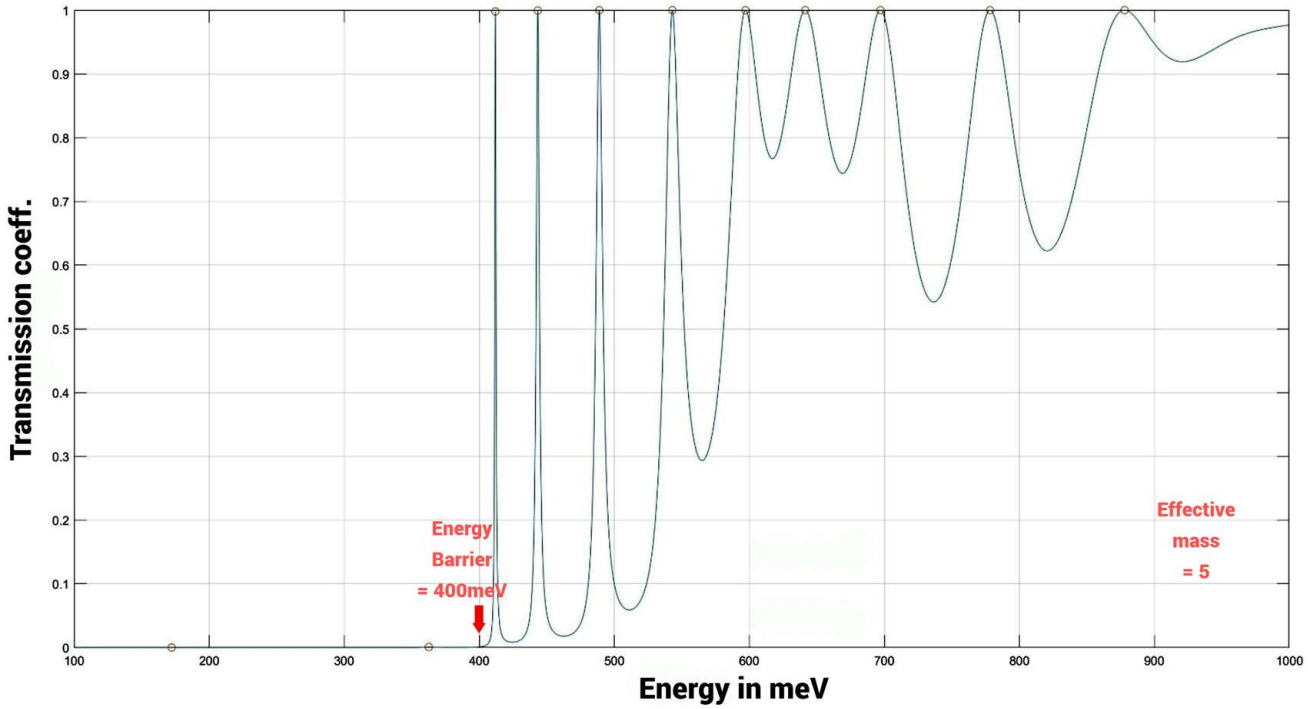

Figure 8. Computer simulation of transmission coeff. vs. energy for different DNA lengths: (**a**) ACGCAGCGT, (**b**) ACGCATGCGT, (**c**) ACGCATAGCGT, (**d**) ACGC$(AT)_2$GCGT, (**e**) ACGC$(AT)_2$AGCGT, (**f**) ACGC$(AT)_3$GCGT, and (**g**) ACGC$(AT)_4$GCGT; quantum barrier = 400 meV and electron effective mass = 5.

The computation results of the quantum well model for different DNA length samples show that the prediction appears to be valid in both the tunneling regime and the hopping regime (unconfined region). For DNA with the inserted A, AT, ATA, or ATAT as a barrier in the middle of A$(CG)_3$T, the experimental results of a large Seebeck coefficient (S: 5 to 7.9 μVK^{-1}) agree with this quantum well model of transmission peaks regarding the tunneling effect within the quantum well regions formed by the barriers. For DNA with the inserted AT base pairs > 4 as a barrier in the middle of A$(CG)_3$T, the experimental results of a smaller Seebeck coefficient (S: 4.9 to 2 μVK^{-1}) also agree with this quantum well model of transmission peaks regarding the hopping transport above the barriers. Figure 8f,g show that there are only narrow transmission peaks with t = 1 appearing above the barrier of E > 400 meV, while there are no transmission peaks for E < 400 meV. These results demonstrate agreement between the experiments [1] and the simulation of varying the AT block combinations for the charge transfer of both tunneling and hopping in the DNA sequences. This agreement and application will be further discussed in Section 5.

3.5. Experimental Validation of the Model in Semiconductor Superlattice Sequences

Aperiodic (or quasiperiodic) quantum wells in a superlattice structure can produce resonance states resembling bound states inside the quantum well [30]. The sequence of the aperiodic quantum well, generated by certain mathematical equations, modulates the unconfined region or above-barrier region, resulting in energy states with very narrow peaks in the transmission coefficient spectrum. Unlike periodic quantum wells, which produce broader peaks, narrow peaks in aperiodic quantum wells show increased carrier stability during traversal in the above-barrier region. When a carrier enters the unconfined region of a quantum well system with a transmission coefficient equal to unity, the corresponding unconfined energy state adopts a resonance state. The "quasibound" resonant

state above the quantum well behaves similarly to bound states inside the quantum well. According to the Uncertainty Principle [31] of $\delta t \delta E \sim h$, the discrete-like energy state above the quantum wells can persist in the energy state used for charge transfer longer than those in other energy states with smaller transmission coefficients and broader peaks. Studies of resonant states in quantum wells and barriers show that transmission coefficient patterns with narrow peaks or smaller bandwidths have physical significance in superlattice semiconductors.

Additionally, experimental techniques, specifically photoreflectance spectroscopy (Appendix A) were used to investigate optical transitions between unconfined states in different superlattice systems [21]. The spectra results reveal that these transitions are significantly enhanced in Fibonacci superlattices and some aperiodic superlattices compared to periodic and random systems of a similar composition. The experimental results are then compared with transition energies computed using the quantum well transfer matrix technique to obtain the transmission coefficients in different energy states. When the transmission coefficient peaks are narrow and approach 1, the charge transfer of the carriers was found to have also increased. The same computational method was used to calculate the functionality of the charge transfer in DNA systems.

4. Discussion

The investigation of charge transfer and transport mechanisms in molecular DNA structures and nanoelectronic devices can lead to a greater understanding of their communication processes. However, environmental and chemical factors give rise to many challenges that affect carrier motion in communication for short-range and long-range charge transport. Minimizing the known factors affecting the physical sequences, I propose that quantum well (QW) analysis be applied to the unconfined region of nanostructures for both periodic and quasiperiodic systems. The quantum well semiconductor superlattice is typically on the scale of nm, about ten times the DNA unit, where a similar application of Quantum Mechanics can be found. By focusing on quasiperiodic sequences and comparing them with the periodic and random sequences of quantum well structures in superlattices, the unconfined states are verified through experiments (see Appendix A) to enhance charge transfer and transport [30]. The quantum well Transfer Matrix Method (TMM) was used to demonstrate that the basic model facilitates the computational process of the transmission coefficient and the corresponding energy positions of transitions. Similar approaches can be used to compare and model different sequences of DNA. The computer simulation presented here is just a starting point to provide more future experiments to calibrate and refine the model, such as the variation of the effective mass of the carrier. This assumes that the environmental and chemical factors influencing charge transfer (CT) can be stabilized and maintained in a constant state. The stability condition allows for the comparison of relative CT values among different types of sequences.

Quantum wells in a superlattice can simplify the investigation of similar sequences in DNA, which have more variance in factors that can influence the outcomes. Cross-checking and optimizing beforehand can complement the results of using DNA molecules. Compared with DNA sequences, the quasiperiodic sequence of non-periodic and non-random arrangements can be generated in a semiconductor superlattice to investigate whether certain DNA sequences can impact the characteristics of CT. Many factors (e.g., aqueousness, counterions, extraction process, electrodes, purity, substrate, structural fluctuations, geometry) influence carrier motion along DNA. These factors are either intrinsic or extrinsic. Here, the focus is on the most important intrinsic factors, i.e., the effect of alternating the base-pair sequence, which affects the overlaps across the π-stacked base pairs. The aim of this work is a comparative examination of the influence of base-pair sequences on CT in aperiodic and quasiperiodic sequences [24].

Utilizing theoretical analysis for the unconfined region of superlattices, a similar investigational model is applied to simulate the transmission coefficient spectrum for the unconfined region in DNA sequences, with the analysis to be verified through experiments

presented in this paper. Both the presence and absence of water have been demonstrated to influence the band structure of DNA base stacks. However, the primary goal of computational studies is to understand the impact of different DNA sequences on CT within the DNA. The simulated results of DNA sequences providing enhanced CT functions are proposed for use in future experiments. The verification and further studies of different aperiodic DNA sequences will offer more insights into DNA CT and optimizing electronic transfer rates concerning energy states in the above-barrier unconfined regions of the QW.

Based on the agreement between this quantum well model and the experimental studies by Li et al. [1], my hypothesis is that transmission peak simulation is an effective tool to supplement the analysis utilizing the hopping mechanism and other transport theories [32] in DNA sequences. The application of TMM can be employed not only for a few DNA base pairs but also for thousands or more base pairs, such as those in the human genome. The computation time is usually less than 1 min, depending on the type of computer used. The complexity of the quantum well model can also be expanded to include extrinsic factors, further increasing the computation time. The transmission peaks and their bandwidths in the transmission coefficient simulation can correlate with the tunneling/hopping resistance and thermoelectric effect in DNA molecules. The following steps can be used to obtain optimized DNA sequences that facilitate CT between the donor and acceptor of the carrier, proceeding through the fastest pathway available in the unconfined region for longer-range DNA CT:

(1) Utilize the quantum well model presented here for simulation to obtain the transmission coefficient vs. energy for different quasiperiodic and random sequences of quantum well nanostructures.
(2) Select narrower bandwidths that produce a transmission peak = 1 as the criterion for choosing optimal sequences in DNA and superlattices.
(3) Build both superlattices and DNA for the samples below (3a and 3b) or, if resources for step 3a are not available, build the samples based on step 3b.
    a. Construct the quantum well superlattice (see examples in Appendix A) according to step 2 and use Photoreflectance or other techniques to identify quantum well sequences with optimal CT characteristics.
    b. Prepare DNA molecules (see the example studies by Li et al. [1]) according to step 2 and use STM, conductivity measurement, or other techniques to identify the quantum well sequences with the best CT characteristics. Measure the hopping resistance and Seebeck coefficient to determine which DNA sequences have the smallest values or cause the thermoelectric effect to become negligible.
(4) Systematically study the above steps and use the experimental results as feedback to optimize the quantum well model and its simulation based on empirical values of the effective mass, barrier height and other related parameters.

The advantages of the above studies are the application of the validated quantum well model for the intrinsic characteristics of DNA molecules with different sequences and lengths, leading to effective approaches to search for sequences optimized for CT in nanostructures. The examples in Appendix A demonstrate that quantum well sequencing has a special influence on the unconfined states in quantum mechanics. I have simulated hundreds to thousands of different combinations of sequences to choose the Thue–Morse and Fibonacci sequences as appropriate sequences to be built into actual superlattices [30]. These quasiperiodic sequences have unique mirror-like symmetry at certain locations and may be suitable for facilitating CT in DNA molecules. The double-stranded structure in DNA runs in opposite directions to each other and is thus antiparallel. Studies of Thue–Morse sequences of DNA with antiparallel characteristics can provide more insight into CT behaviors.

Other compelling studies [33] by Xiang et al. include applying an electrochemical (EC) gate voltage to a DNA molecule, leading to the reversible switching of DNA conductance between two discrete levels. Only basic DNA sequences were used in the experiments

together with theoretical calculations to demonstrate the change in energy level switching related to the Fermi level of the contact electrodes. In this study, I propose different quasiperiodic DNA sequences that can undergo similar tests and experiments. The Electromodulation spectra of Thue–Morse superlattice with different modulating voltages are shown in Figure A2 of Appendix A. The different levels of carrier states in the unconfined region increase when the modulating voltage is increased. Along with similar research goals, studies of Thue–Morse sequences of DNA with different EC gate voltages can provide more insight into CT behaviors. In particular, quantum computers require sophisticated nanostructures to carry out quantum computing. Controlling the switching of different levels effectively with less energy consumption also requires a high CT rate in the unconfined region of quantum wells. Therefore, the proposed Thue–Morse sequence could be a candidate that meets the demands of quantum computing.

Recent advancements in DNA technology have led to the construction of innovative nanoscale structures such as DNA origami, a technique that involves folding a long DNA strand into predefined shapes. This method has been applied to create three-dimensional DNA-programmable nanoparticle superlattices [26]. Researchers [18,19,34–37] have combined DNA-based assembly with lithography to fabricate reconfigurable nanoparticle structures on gold surfaces. By using specific DNA sequences and polymer pores, the arrangement of nanoparticles can be precisely controlled, resulting in highly ordered structures with tunable distances between particles [34]. These unique DNA sequence designs give rise to further functionality for advanced technologies like biosensors [38,39], microelectronics, nanosuperconductors [40], and semiconductor devices.

Finally, I want to draw attention to my studies of DNA simulation and nanostructures/superlattices using the quantum well model, which can provide synergy with the latest developments in real-world applications. I use a paper titled, "Building superlattices from individual nanoparticles via template-confined DNA-mediated assembly" * as an illustration. The paper details a method for arranging nanoparticles into precise structures on a surface using electron-beam lithography and DNA-mediated assembly. First, a layer of poly(methyl methacrylate) (PMMA) with tiny pores is patterned onto a gold-coated silicon surface. The gold at the bottom of each pore is then coated with DNA sequences, and complementary DNA-modified gold nanoparticles are added, building up layers in a specific order using the "sticky ends" of DNA and modified "locked" DNA bases [19]. This technique can generate uniform superlattices of nanoparticles in different layers. Even though the experiments recorded in the supplemental material (my PhD thesis) are 1-D superlattices and use different materials, the investigation of mathematical sequences can shine light in the direction of furthering the studies in the following proposals:

(1) Referring to the paper's processing steps for "gold at the bottom of each pore is then coated with DNA sequences", these sequences can be Fibonacci, Thue–Morse, and other DNA sequences with different layers, as shown in my simulations.
(2) The generality and functionality of this integration will be explored by identifying broadband absorption with a solvent polarity response that allows dynamic tuning of the distance between nanoparticles. The new DNA sequence design, together with the robust structures made by the new DNA-mediated assembly techniques, will advance technologies in biosensors, microelectronics, and semiconductor devices.
(3) Photoreflectance studies have the potential to be used to study these three-dimensional superlattices when proper selection of materials in a semiconductor superlattice and DNA-mediated assembly are investigated and optimized.
(4) The first 44 boundaries of the Fibonacci sequenced DNA correspond to the first symmetric sequence, i.e., the left half sequence is the mirror image of the right half sequence. This appears to be the criterion for generating a unity transmission peak. At the other boundaries, one or more units in the sequence do not meet the mirror image requirement, which could result in a reduced transmission peak. However, the corresponding position of the transitions remains the same even though the number of boundaries is changed. This preservation of the transmission coefficient of

aperiodic superlattices is especially advantageous in the study of optical transitions. This, therefore, gives rise to consistent transition energies among the peaks of the transmission coefficients, in which the combined effect can increase the total transition strength. When the transmission coefficient peaks are narrow and approach 1, the charge transfer of the carriers was found to have also increased, as demonstrated in Section 3.5.

(5) The optical transition strengths of the unconfined states were enhanced for Thue–Morse sequenced DNA and superlattices when compared with samples having periodic or random sequences. The alignment of the unconfined states in different types of DNA-mediated assemblies and superlattices could be yet another interesting area for further exploration and investigation.

(6) This study of aperiodic DNA and superlattices assumes, essentially, a one-dimensional structure. This approach, however, could be extended to a study of other aperiodic systems using three-dimensional structures such as quasiperiodic DNA and superlattices. The majority of the latest research on the self-assembly of DNA nanoparticles is related to the formation of diverse 2D periodic nanopatterns [41], such as tetragonal, hexagonal, rectangular, and oblique structures. There is a need for more explorations in aperiodic nanoparticles, where, for instance, fivefold symmetry [42] in an X-ray diffraction pattern has been seen only in quasiperiodic crystals [43] which are related to the Fibonacci sequence [44]. It would be impossible to generate such patterns with regular, periodic crystals. This research work lays a foundation for exploring the physical behaviors of unconfined states in aperiodic DNA and superlattices. New characteristics and new applications can be discovered when further investigation of aperiodic systems continues.

The Fibonacci sequences and related ratios were also found to have an interesting connection with the nucleotide frequencies in single-stranded DNA of the human genome [45–47]. Investigation of the golden ratio 1.618 and quasiperiodic sequences in nature can provide insight into some of the physical characteristics of aperiodic systems. Although studies of the quantum walk on protein-DNA target search [48] and in an aperiodic space-inhomogeneous system can provide insight into localization properties and enhancement of entanglement [49] in quantum systems, the quantum well model presented in this study can facilitate and complement the investigation of DNA interaction and nanoelectronics.

5. Conclusions

In conclusion, we have conducted theoretical studies using the quantum well model on the quasiperiodic sequences of Fibonacci and Thue–Morse samples for DNA nanostructures. Previous experimental results were used to validate the quantum well model in DNA molecules and semiconductor superlattices.

Compared with the periodic and random samples, the Fibonacci and Thue–Morse samples enhance the unconfined transitions by an order of magnitude in strength (Figures A1 and A2 in Appendix A of semiconductor superlattices). The experimental results agreed with the quantum well model simulation and provide a foundation on which to expand the application into DNA nanostructures, which have dimensions of about an order of magnitude smaller than those of superlattices. The same quantum well model and computational method were applied to the quasiperiodic sequences of Fibonacci and Thue–Morse samples for DNA nanostructures. An effective mass value of 5 was selected for the carrier (electron or hole) transfer in the simulations, as shown in Figures 4–6. When changing the effective mass values, the simulation results of transmission peaks can be shifted. A more accurate determination of the effective mass value in DNA nanostructures will improve the simulation results when compared with the experimental results. The study on the thermoelectric effect and its dependence on molecular length and sequence in single DNA molecules [1] was used to compare the simulations using the quantum well model. The results demonstrate agreement and provide new insights into charge transfer and transport

in DNA nanostructures with various sequences. Further experiments and analysis are needed to gain more insight and understanding of the characteristics of the Fibonacci and Thue–Morse sequences in DNA.

The cellular diagnostic mechanism [32,50] using DNA charge transfer (CT) assists in scanning the genome to localize the damage and mutational sites, which helps bring in the DNA repair protein. This process can prevent uncontrolled mutations and improve cancer treatment. Studying quantum mechanical effects and efficient communication across DNA can provide more insights into disease healing. Additionally, the theoretical analysis, computer simulation, and experimental results of quasiperiodic quantum systems can be applied to the development of nanoelectronic circuits for quantum computing, information storage [51,52], and other quantum devices [17].

Semiconductors, the backbone of modern computing, rely on controlled charge transfer, where charge carriers (electrons or holes) move across materials with an applied voltage, enabling the functioning of transistors, diodes, and other electronic components. The integration of DNA with semiconductor technology opens possibilities for creating biocompatible computing devices that operate at the nanoscale. These studies have the potential to revolutionize computing by integrating biological molecules into electronic circuits, paving the way for innovations in bioelectronics and nanodevices [53]. By controlling factors such as temperature, chemical processes, and DNA sequences, researchers can explore the potential of DNA in various electronic applications. Thus, the exploration of DNA charge transfer and transport with different mathematical sequences proposed by this research paper is not only a fundamental scientific endeavor but also a pathway toward innovative technological applications in quantum computing and biotechnology.

Despite significant progress in DNA research since its discovery [54], much remains to be explored about the characteristics of DNA sequences [15,55–57]. The material world, from atoms to stars, predominantly exhibits periodic structures. However, the DNA of life on Earth consists largely of aperiodic structures that not only store genetic information but also relate to the efficiency of charge transfer within DNA. Understanding the impact of aperiodic DNA sequences on life requires fundamental knowledge of the basic mathematical sequences of DNA. The more we learn from this essential investigation, the more we can piece together the puzzle that reveals the entire picture of the mystery of DNA.

Supplementary Materials: The following supporting information can be downloaded at: https://www.mdpi.com/article/10.3390/biophysica4030027/s1.

Funding: No external funding was provided for this research. It is primarily driven by my eagerness to learn and my curiosity about nature. I personally financed this research and its publication out of my passion for fundamental scientific research and to understand how DNA sequences impact biological life. After completing my Ph.D. research on "The Study of Unconfined States in Quasi-Periodic Semiconductor Superlattices" at Boston College, I worked in various medical device companies, saving funds until my recent retirement. I am now an Adjunct Professor of Physics at Grand Canyon University in Arizona and an independent researcher, expanding my investigation from semiconductor superlattices to nanostructures with different aperiodic DNA sequences.

Data Availability Statement: The data presented in this study are available in the main text, references and the Supplementary Materials.

Acknowledgments: I would like to thank M. Graf, D. Broido, P. Bakshi, K. Kempa for their helpful discussions and the staff at Boston College and Grand Canyon University for their support in administration. Special thanks to T. Moustakas and T. Chiu for their efforts in growing high-quality superlattices for the experiments. I am grateful to my late advisor, G. Goldsmith, for his guidance and mentorship during my Ph.D. research in quantum physics. I also appreciate the comments and feedback from Breanna Tai (+grammar editor), Victoria Tai, Kayi Chan and Manni Mo. Finally, I thank God for the goodness and grace that have inspired and motivated me to contribute to science and life.

Conflicts of Interest: The author declares no conflicts of interest.

Appendix A

We review some of the previous work [30] on the experimental techniques of photoreflectance spectroscopy used to investigate the optical transitions between unconfined states in various superlattice systems. The experimental results are compared with transition energies computed by the quantum well Transfer Matrix Method (TMM) to obtain transmission coefficients in different energy states. When the transmission coefficient peaks are narrow and approaching 1, the charge transfer of the carriers is increased. The same computational method was used to calculate the functionality of charge transfer in the DNA systems.

Three different superlattice samples [58] were grown on GaAs substrates in the (100) orientation using a VG-V80H MBE system under similar growth conditions:

(i) Periodic, with alternating layers of AlGaAs (A) and GaAs (B);
(ii) Quasiperiodic, with layers deposited according to the Fibonacci sequence;
(iii) Random, with layers A and B selected by a random-number generator.

In all samples, the Al mole fraction, x, = 0.3; the AlGaAs (A) barrier width = 40 Å; and the GaAs (B) well width = 28.3 Å. In each instance, the total of barrier and well widths are made up of 600 layers (either A or B), resulting in a film thickness of approximately 2 μm. The periodic sample was prepared to serve as a comparison with the other samples.

To build relations between the charge transfer of a superlattice semiconductor and DNA, a one-dimensional sequence with 1 or 0 will be used to simulate the sequence of a quantum well and barrier, respectively. The superlattice samples were prepared on GaAs (undoped) substrates using an MBE system with the basic unit length of an AlGaAs barrier (0) = 40 Å, and that of a GaAs well (1) = 28.3 Å. In contrast, the helical chains of nucleotides in DNA are bound to each other by hydrogen bonds that coil into tight loops and form different shapes of polymers.

The existence of localized unconfined energy states in multiple periodic GaAs-AlGaAs quantum wells has been observed by photoluminescence spectra [59] and by photoreflectance spectroscopy [60]. Several material and system parameters were found to influence the transition probability within the unconfined regions. In the periodic GaAs-AlGaAs system, for example, wider barrier widths [59] and smaller Al mole fraction [60] have been found to enhance these transitions. Similar studies, however, of the unconfined energy states in the quasiperiodic and random quantum well structures have not received much attention [61]. The optical transitions involving the unconfined states of GaAs-AlGaAs in quasiperiodic, periodic, and random superlattices are compared. In the random superlattice, the well widths and/or the barrier widths are varied according to an arbitrary random pattern. In contrast, the Fibonacci superlattice [62] is made up of an arrangement of layers of type A and type B following the Fibonacci sequence S1 = A, S2 = B, S3 = AB, S4 = BAB,. . . , Si = (Si − 2)(Si − 1). This leads to a quasiperiodic sequence of wells and barriers. Its band structure and wavefunction localization in the confined states region have been shown to be dependent on the order of quasiperiodic modulation.

Photoreflectance is an optical and contactless technique for investigating the material and electronic properties of thin films that include semiconductor multiple quantum wells. Photoreflectance uses periodic pulses of strongly absorbed light (“pump” beam) to excite electron-hole pairs, which, upon diffusion, create a field in the sample modifying the dielectric function synchronously with the optical excitation. Simultaneously, the sample is scanned spectrally with a “probe” beam. Synchronous detection of the reflected (or transmitted) probe light separates the modulated signal from the strongly reflected (or transmitted) steady-state background, resulting in greatly improved spectral contrast compared to that of the static reflection or transmission spectrum. It measures the change in reflectivity of a sample in response to the application of an amplitude-modulated light beam. In general, a photo-reflectometer consists of an intensity-modulated “pump” light beam used to modulate the reflectivity of the sample, a second “probe” light beam used to measure the reflectance of the sample, an optical system for directing the pump and probe beams to the sample, and for directing the reflected probe light onto a photodetector, and a

signal processor to record the differential reflectance. The pump light is typically modulated at a known frequency so that a lock-in amplifier may be used to suppress unwanted noise, resulting in the ability to detect reflectance changes at the ppm level. Both experimental and theoretical details of the photoreflectance technique may be found in several review papers and books, the most comprehensive of which is "Modulation Spectroscopy" by M. Cardona [63]. Pollak et al. used photoreflectance to characterize the interband transitions in GaAs-GaAlAs multiple quantum wells [64]. From their observations of the line widths of the transition, they obtained direct information concerning the Al content and the width and quality of the multiple quantum well structure.

As shown in Figure A1a, only weak transitions are observed in the unconfined region for the periodic sample. In Figure A1b, two conspicuous features appear in the unconfined region for the Fibonacci superlattices. In Figure A1c, overlapping features are observed, with the unconfined transition magnitude lying between those of periodic and Fibonacci superlattices for the random superlattices.

The corresponding computed results [30] were compared with the experimental results, and they agree well, indicating:

(i) Periodic sample: A wide gap appears between the top of the barrier and the first unconfined energy band above the barrier;
(ii) Fibonacci sample: Distinct features of the unconfined states appear very close to the barrier;
(iii) Random samples: Overlapping features of unconfined states appeared above the barrier.

The strong signals obtained in the unconfined region of the Fibonacci sample observed in the photoreflectance spectra match with the theoretical calculation. The narrow energy bandwidth corresponding to the unconfined transition implies a longer time spent in the well due to the uncertainty principle. The longer time the electron spends in the well, the higher the probabilities for the electron to be captured by the well. Therefore, the transition strength is enhanced. The Anderson localization [65] effect shows that the wavefunctions form the wave packet to become a localized state. The carrier transport efficiency decreases along the growth axis of purposely disordered or random GaAs/GaAlAs superlattices. On the other hand, the carrier transport efficiency increases when the bandwidth of the transmission peaks is distinct and narrow in the simulation of the Fibonacci sample. The large signals of "A" and "B" in Figure A1b validate the theory and simulation of this study. When compared with the periodic and random samples, the Fibonacci sample enhances the unconfined transitions by an order of magnitude in strength.

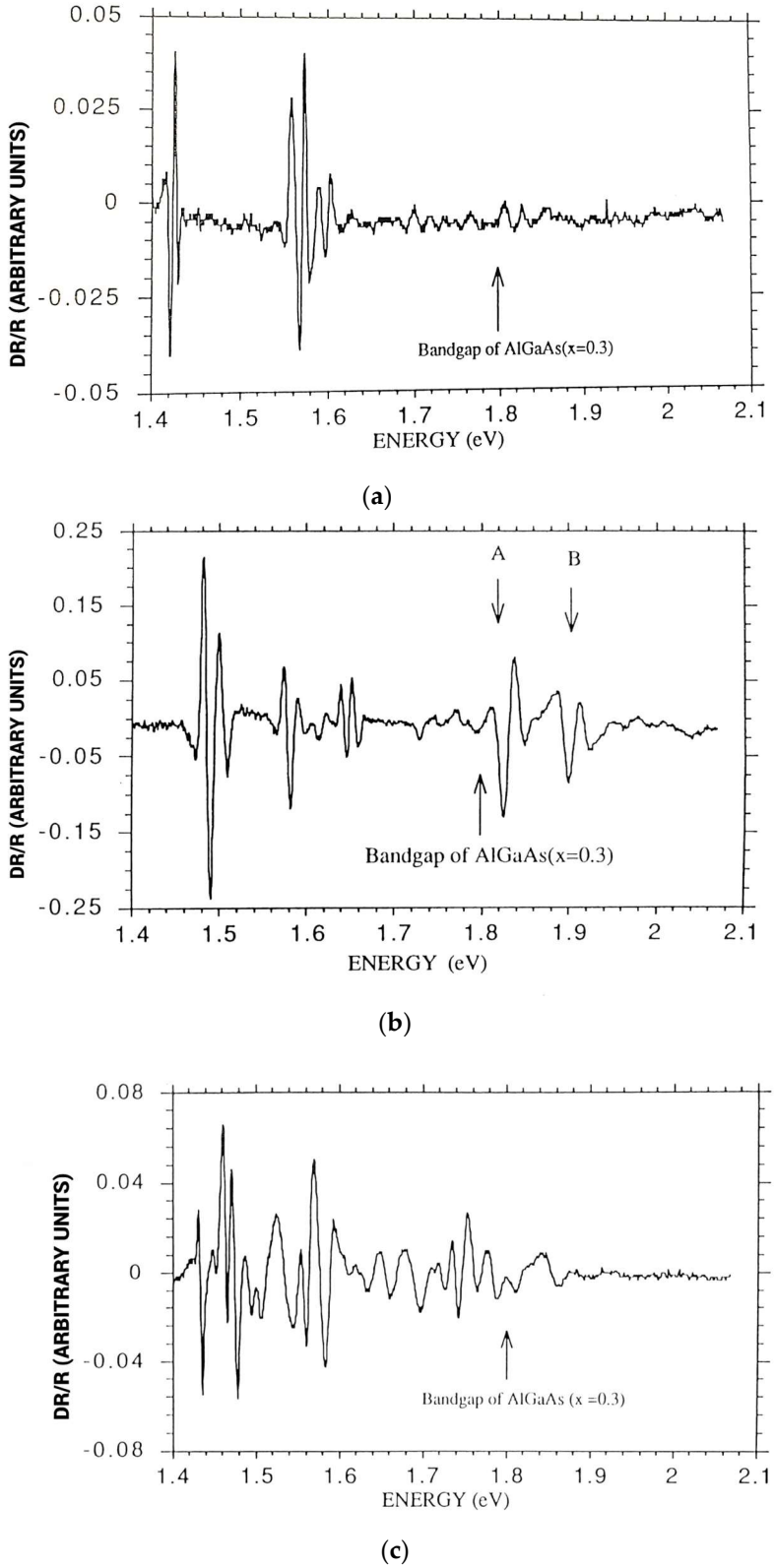

Figure A1. Photoreflectance spectra of (**a**) periodic, (**b**) Fibonacci, and (**c**) random superlattices at room temperature.

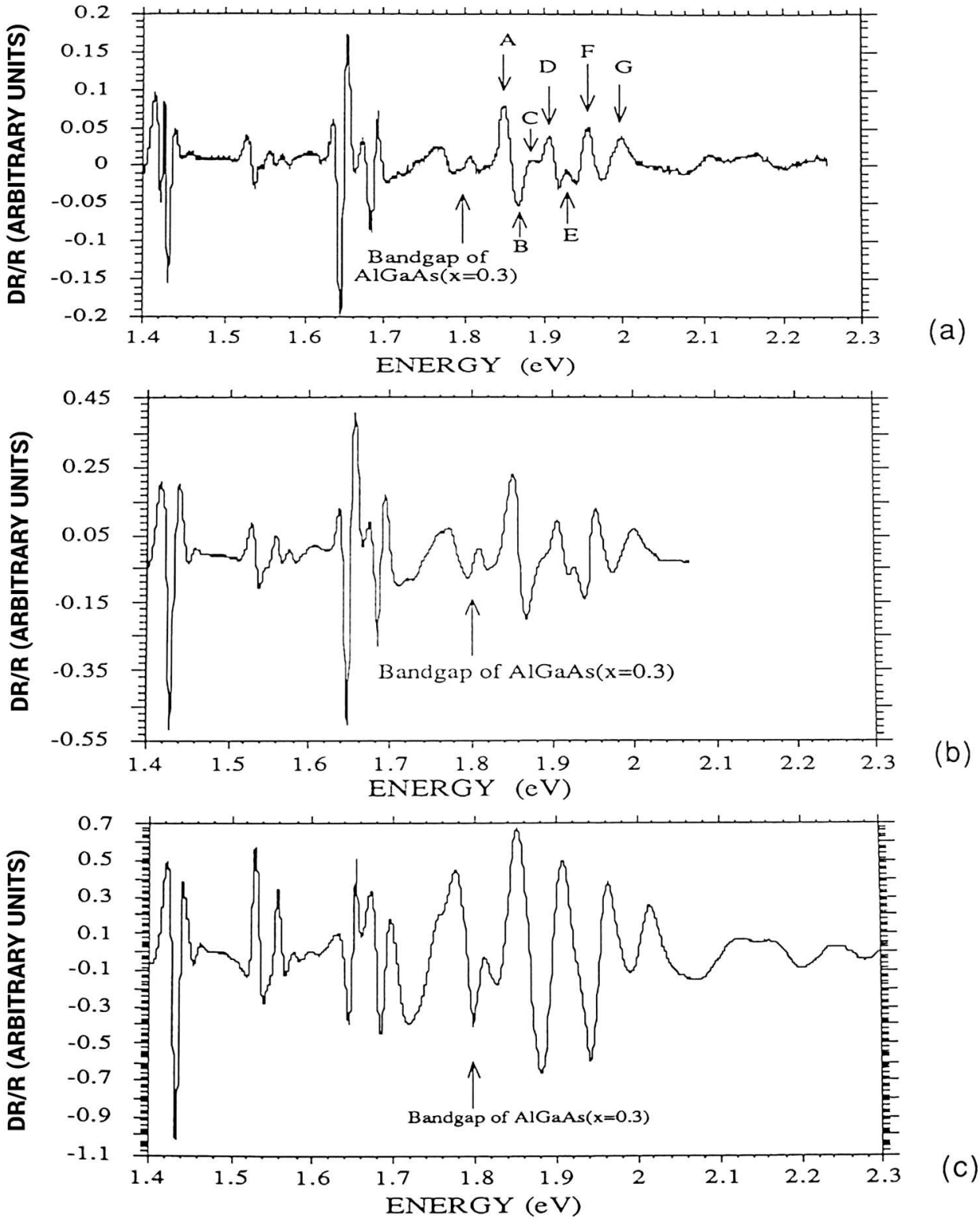

Figure A2. Electromodulation spectra of Thue–Morse superlattice with modulating voltage at (**a**) 4Vp-p, (**b**) 10Vp-p, and (**c**) 20Vp-p. The measurements were performed at room temperature with the bias at 0 V.

The transmission peak is sensitive to the number of layers considered in the calculation. For the quasiperiodic superlattice (Fibonacci sequence, Table 2), the general patterns remain the same when the number of boundaries is changed. In particular, the superlattice with 44 boundaries has unity transmission peaks, while the others do not quite have these

unity transmission peaks. The resolution of the calculated transmission coefficients is the same and equal to 0.1 meV. We find that the 44 boundaries of the Fibonacci superlattice correspond to the first symmetric sequence, i.e., the half-left sequence is the image of the half-right sequence. This is the criterion for generating a unity transmission peak. At the other boundaries, the half-left sequences do not form a perfect mirror image of the corresponding half-right sequence. There exist one or more units in the sequence that do not match the image requirement. These result in generating transmission peaks less than unity besides the slight shift of their energy position. These can be further supported by the transmission plot in the "Thue-Morse" superlattice (Table 3). The sequence that forms the superlattice meets the image matching requirement at layers 1 to 64. This results in unity transmission peaks. Another image matching occurs at layers 1 to 256 (172 boundaries), which give rise to unity transmission peaks in the simulations (Figure 6b). These are some of the characteristics of quasiperiodic superlattices that cannot be found in random superlattices. This preservation of the transmission coefficient of quasiperiodic superlattices is especially advantageous for the study of optical transitions [66–68] and transport properties [69,70]. The corresponding positions of the transitions remain the same even though the penetration depth of the probe and pump light is changed, i.e., the number of layers is changed. Therefore, this gives rise to consistent transition energy, in which the combined effect can increase the transition strength.

The unconfined state transition of the superlattices belongs to the band-to-band transition. Hence, the application of a large electric field can generate the Franz-Keldysh effect [71]. The depletion layer of the superlattice is estimated to be in the order of 10,000 Å. The strength of the electric field is in the order of 106 V/m when 10 V is applied across the sample. This large electric field can result in the Franz-Keldysh effect. As shown in Figure A2a–c, the relative amplitude of the unconfined transition signal to the GaAs signal of the Thue–Morse superlattice increases almost two-fold when the modulation voltage increases from 4Vp-p to 20Vp-p. There are six peaks in the unconfined region at 4Vp-p. While the voltage increases, two of the peaks shrink and the total peaks end up in four large peaks at 20Vp-p. The unconfined state transition strengths were enhanced for the quasiperiodic sample (Thue–Morse superlattice) when compared with samples having periodic and random sequences. The experimental results of the measured extended transition energies agree qualitatively with theoretical Transfer Matrix (TMM) calculations. Better agreement can be achieved through the application of a more sophisticated multi-band model. Further experiments and analysis will be performed to gain more insight and understanding concerning the characteristics of the Thue–Morse sample with respect to superlattice and DNA nanostructures.

References

1. Li, Y.; Xiang, L.; Palma, J.L.; Asai, Y.; Tao, N. Thermoelectric effect and its dependence on molecular length and sequence in single DNA molecules. *Nat. Commun.* **2016**, *7*, 11294. [CrossRef] [PubMed]
2. Jortner, J.; Bixon, M.; Langenbacher, T.; Michel-Beyerle, M.E. Charge transfer and transport in DNA. *Proc. Natl. Acad. Sci. USA* **1998**, *95*, 12759–12765. [CrossRef] [PubMed]
3. Boon, E.M.; Barton, J.K. Charge transport in DNA. *Curr. Opin. Struct. Biol.* **2002**, *12*, 320–329. [CrossRef]
4. Rawtani, D.; Kuntmal, B.; Agrawal, Y. Charge transfer in DNA and its diverse modelling approaches. *Front. Life Sci.* **2016**, *9*, 214–225. [CrossRef]
5. Iguchi, K. Semiconductivity and Band Gap of a Double Strand of DNA. *J. Phys. Soc. Jpn.* **2001**, *70*, 593–597. [CrossRef]
6. Wang, H.; Lewis, J.P.; Sankey, O.F. Band-Gap Tunneling States in DNA. *Phys. Rev. Lett.* **2004**, *93*, 016401. [CrossRef]
7. Beratan, D.N. Why Are DNA and Protein Electron Transfer So Different? *Annu. Rev. Phys. Chem.* **2019**, *70*, 71–97. [CrossRef]
8. Fujitsuka, M.; Majima, T. Charge transfer dynamics in DNA revealed by time-resolved spectroscopy. *Chem. Sci.* **2017**, *8*, 1752–1762. [CrossRef]
9. Simmons, C.R.; MacCulloch, T.; Krepl, M.; Matthies, M.; Buchberger, A.; Crawford, I.; Šponer, J.; Šulc, P.; Stephanopoulos, N.; Yan, H. The influence of holliday junction sequence and dynamics on DNA crystal self-assembly. *Nat. Commun.* **2022**, *13*, 3112. [CrossRef]
10. Yudiarsah, E. I-V characteristic of Poly(dA)-poly(dT) DNA molecule: The role of internal electric field. *J. Phys. Conf. Ser.* **2021**, *1816*, 012060. [CrossRef]

11. Deffner, M.; Weise, M.P.; Zhang, H.; Mücke, M.; Proppe, J.; Franco, I.; Herrmann, C. Learning Conductance: Gaussian Process Regression for Molecular Electronics. *J. Chem. Theory Comput.* **2023**, *19*, 992–1002. [CrossRef] [PubMed]
12. Korol, R.; Segal, D. Machine Learning Prediction of DNA Charge Transport. *J. Phys. Chem. B* **2019**, *123*, 2801–2811. [CrossRef] [PubMed]
13. Zhou, X.; Lin, S.; Yan, H. Interfacing DNA nanotechnology and biomimetic photonic complexes: Advances and prospects in energy and biomedicine. *J. Nanobiotechnol.* **2022**, *20*, 257. [CrossRef] [PubMed]
14. Schrodinger, E. *What Is Life?: With Mind and Matter and Autobiographical Sketches*; Cambridge University Press: Cambridge, UK, 2012.
15. Bormashenko, E. Fibonacci Sequences, Symmetry and Order in Biological Patterns, Their Sources, Information Origin and the Landauer Principle. *Biophysica* **2022**, *2*, 292–307. [CrossRef]
16. Roche, S.; Maciá, E. Electronic transport and thermopower in aperiodic dna sequences. *Mod. Phys. Lett. B* **2004**, *18*, 847–871. [CrossRef]
17. Maciá, E. The role of aperiodic order in science and technology. *Rep. Prog. Phys.* **2005**, *69*, 397. [CrossRef]
18. Julin, S.; Nummelin, S.; Kostiainen, M.A.; Linko, V. DNA nanostructure-directed assembly of metal nanoparticle superlattices. *J. Nanoparticle Res.* **2018**, *20*, 119. [CrossRef]
19. Lin, Q.-Y.; Mason, J.A.; Li, Z.; Zhou, W.; O'Brien, M.N.; Brown, K.A.; Jones, M.R.; Butun, S.; Lee, B.; Dravid, V.P.; et al. Building superlattices from individual nanoparticles via template-confined DNA-mediated assembly. *Science* **2018**, *359*, 669–672. [CrossRef]
20. Barnaby, S.N.; Thaner, R.V.; Ross, M.B.; Brown, K.A.; Schatz, G.C.; Mirkin, C.A. Modular and Chemically Responsive Oligonucleotide "Bonds" in Nanoparticle Superlattices. *J. Am. Chem. Soc.* **2015**, *137*, 13566–13571. [CrossRef]
21. Ferreira, R.; Bastard, G. Unbound states in quantum heterostructures. *Nanoscale Res. Lett.* **2006**, *1*, 120–136. [CrossRef]
22. Austin, E.J.; Jaros, M. Electronic structure and transport properties of GaAs-GaAlAs superlattices in high perpendicular electric fields. *J. Appl. Phys.* **1987**, *62*, 558–564. [CrossRef]
23. Lent, C.S.; Porod, W. Effect of continuum resonances on electronic transport in quantum wells. *Superlattices Microstruct.* **1988**, *4*, 77–80. [CrossRef]
24. Mantela, M.; Lambropoulos, K.; Theodorakou, M.; Simserides, C. Quasi-Periodic and Fractal Polymers: Energy Structure and Carrier Transfer. *Materials* **2019**, *12*, 2177. [CrossRef]
25. Grodick, M.A. DNA-Mediated Charge Transport Signaling Within the Cell. Ph.D. Thesis, California Institute of Technology, Pasadena, CA, USA, 2016.
26. Kahn, J.S.; Minevich, B.; Gang, O. Three-dimensional DNA-programmable nanoparticle superlattices. *Curr. Opin. Biotechnol.* **2020**, *63*, 142–150. [CrossRef] [PubMed]
27. Edirisinghe Pathirannehelage, N. Charge Transfer in Deoxyribonucleic Acid (DNA): Static Disorder, Dynamic Fluctuations and Complex Kinetic. Ph.D. Thesis, Georgia State University, Atlanta, GA, USA, 2011.
28. Maia, F.F.; Freire, V.N.; Caetano, E.W.S.; Azevedo, D.L.; Sales, F.A.M.; Albuquerque, E.L. Anhydrous crystals of DNA bases are wide gap semiconductors. *J. Chem. Phys.* **2011**, *134*, 175101. [CrossRef] [PubMed]
29. Riklund, R.; Severin, M.; Liu, Y. The thue-morse aperiodic crystal, a link between the fibonacci quasicrystal and the periodic crystal. *Int. J. Mod. Phys. B* **1987**, *1*, 121–132. [CrossRef]
30. Tai, A.C.-C. Study of Unconfined States in Quasi-Periodic Semiconductor Superlattices. Ph.D. Thesis, Boston College, Chestnut Hill, MA, USA, 1991.
31. Blado, G.; Owens, C.; Meyers, V. Quantum wells and the generalized uncertainty principle. *Eur. J. Phys.* **2014**, *35*, 065011. [CrossRef]
32. Genereux, J.C.; Barton, J.K. Mechanisms for DNA Charge Transport. *Chem. Rev.* **2010**, *110*, 1642–1662. [CrossRef]
33. Xiang, L.; Palma, J.L.; Li, Y.; Mujica, V.; Ratner, M.A.; Tao, N. Gate-controlled conductance switching in DNA. *Nat. Commun.* **2017**, *8*, 14471. [CrossRef]
34. Howorka, S. DNA Nanoarchitectonics: Assembled DNA at Interfaces. *Langmuir* **2013**, *29*, 7344–7353. [CrossRef]
35. Li, Y.; Jin, H.; Zhou, W.; Wang, Z.; Lin, Z.; Mirkin, C.A.; Espinosa, H.D. Ultrastrong colloidal crystal metamaterials engineered with DNA. *Sci. Adv.* **2023**, *9*, eadj8103. [CrossRef]
36. Michelson, A.; Subramanian, A.; Kisslinger, K.; Tiwale, N.; Xiang, S.; Shen, E.; Kahn, J.S.; Nykypanchuk, D.; Yan, H.; Nam, C.-Y.; et al. Three-dimensional nanoscale metal, metal oxide, and semiconductor frameworks through DNA-programmable assembly and templating. *Sci. Adv.* **2024**, *10*, eadl0604. [CrossRef] [PubMed]
37. Majewski, P.W.; Michelson, A.; Cordeiro, M.A.L.; Tian, C.; Ma, C.; Kisslinger, K.; Tian, Y.; Liu, W.; Stach, E.A.; Yager, K.G.; et al. Resilient three-dimensional ordered architectures assembled from nanoparticles by DNA. *Sci. Adv.* **2021**, *7*, eabf0617. [CrossRef] [PubMed]
38. Gaba, S.; Chauhan, N.; Chandra, R.; Jain, U. Future advances of artificial biosensor technology in biomedical applications. *Talanta Open* **2024**, *9*, 100301. [CrossRef]
39. Wang, Q.; Wang, J.; Huang, Y.; Du, Y.; Zhang, Y.; Cui, Y.; Kong, D. Development of the DNA-based biosensors for high performance in detection of molecular biomarkers: More rapid, sensitive, and universal. *Biosens. Bioelectron.* **2022**, *197*, 113739. [CrossRef] [PubMed]

40. Shani, L.; Michelson, A.N.; Minevich, B.; Fleger, Y.; Stern, M.; Shaulov, A.; Yeshurun, Y.; Gang, O. DNA-assembled superconducting 3D nanoscale architectures. *Nat. Commun.* **2020**, *11*, 5697. [CrossRef]
41. Hou, B.; Zhang, W.-B.; Shao, Y. Unconventional 2D Periodic Nanopatterns Based on Block Molecules. *Chin. J. Polym. Sci.* **2023**, *41*, 1508–1524. [CrossRef]
42. Sparavigna, A.C.; Baldi, M. Symmetry and the golden ratio in the analysis of a regular pentagon. *Int. J. Math. Educ. Sci. Technol.* **2016**, *48*, 1–11. [CrossRef]
43. Caspar, D.L.D.; Fontano, E. Five-fold symmetry in crystalline quasicrystal lattices. *Proc. Natl. Acad. Sci. USA* **1996**, *93*, 14271–14278. [CrossRef]
44. Jagannathan, A. The Fibonacci quasicrystal: Case study of hidden dimensions and multifractality. *Rev. Mod. Phys.* **2021**, *93*, 045001. [CrossRef]
45. Perez, J.-C. The "3 Genomic Numbers" Discovery: How Our Genome Single-Stranded DNA Sequence Is "Self-Designed" as a Numerical Whole. *Appl. Math.* **2013**, *4*, 37–53. [CrossRef]
46. Perez, J.-C. Codon populations in single-stranded whole human genome DNA Are fractal and fine-tuned by the Golden Ratio 1.618. *Interdiscip. Sci. Comput. Life Sci.* **2010**, *2*, 228–240. [CrossRef] [PubMed]
47. Yamagishi, M.E.B.; Shimabukuro, A.I. Nucleotide frequencies in human genome and fibonacci numbers. *Bull. Math. Biol.* **2008**, *70*, 643–653. [CrossRef] [PubMed]
48. D'Acunto, M. Protein-DNA target search relies on quantum walk. *Biosystems* **2021**, *201*, 104340. [CrossRef]
49. Buarque, A.; Dias, W. Aperiodic space-inhomogeneous quantum walks: Localization properties, energy spectra, and enhancement of entanglement. *Phys. Rev. E* **2019**, *100*, 032106. [CrossRef] [PubMed]
50. Tse, E.C.M.; Zwang, T.J.; Bedoya, S.; Barton, J.K. Effective Distance for DNA-Mediated Charge Transport between Repair Proteins. *ACS Cent. Sci.* **2019**, *5*, 65–72. [CrossRef] [PubMed]
51. Goldman, N.; Bertone, P.; Chen, S.; Dessimoz, C.; LeProust, E.M.; Sipos, B.; Birney, E. Towards practical, high-capacity, low-maintenance information storage in synthesized DNA. *Nature* **2013**, *494*, 77–80. [CrossRef]
52. Preuss, I.; Rosenberg, M.; Yakhini, Z.; Anavy, L. Efficient DNA-based data storage using shortmer combinatorial encoding. *Sci. Rep.* **2024**, *14*, 7731. [CrossRef]
53. Fan, Q.; Yang, L.; Chao, J. Recent Advances in Dynamic DNA Nanodevice. *Chemistry* **2023**, *5*, 1781–1803. [CrossRef]
54. Discovery of DNA Double Helix: Watson and Crick | Learn Science at Scitable. Available online: http://www.nature.com/scitable/topicpage/discovery-of-dna-structure-and-function-watson-397 (accessed on 22 June 2024).
55. Pinho, A.J.; Garcia, S.P.; Pratas, D.; Ferreira, P.J.S.G. DNA Sequences at a Glance. *PLoS ONE* **2013**, *8*, e79922. [CrossRef]
56. Singh, R.; Sophiarani, Y. A report on DNA sequence determinants in gene expression. *Bioinformation* **2020**, *16*, 422–431. [CrossRef]
57. Exploring DNA Sequences. Available online: https://www.labxchange.org/library/items/lb:LabXchange:571811ba:html:1 (accessed on 21 June 2024).
58. Clarke, R.; Moustakas, T.; Bajema, K.; Grier, D.; Dos Passos, W.; Merlin, R. Structural fluctuations and randomness in GaAsAlxGa1-xAs superlattices. *Superlattices Microstruct.* **1988**, *4*, 371–374. [CrossRef]
59. Song, J.J.; Yoon, Y.S.; Fedotowsky, A.; Kim, Y.B.; Schulman, J.N.; Tu, C.W.; Huang, D.; Morkoc, H. Barrier-width dependence of optical transitions involving unconfined energy states in GaAs-AlGaAs superlattices. *Phys. Rev. B* **1986**, *34*, 8958–8962. [CrossRef]
60. Reddy, U.K.; Ji, G.; Henderson, T.; Morkoç, H.; Schulman, J.N. Investigation of GaAs/(Al,Ga)As multiple quantum wells by photoreflectance. *J. Appl. Phys.* **1987**, *62*, 145–151. [CrossRef]
61. Bastard, G.; Ziemelis, U.O.; Delalande, C.; Voos, M.; Gossard, A.C.; Wiegmann, W. Bound and virtual bound states in semiconductor quantum wells. *Solid State Commun.* **1984**, *49*, 671–674. [CrossRef]
62. Merlin, R.; Bajema, K.; Clarke, R.; Juang, F.-Y.; Bhattacharya, P.K. Quasiperiodic GaAs-AlAs Heterostructures. *Phys. Rev. Lett.* **1985**, *55*, 1768–1770. [CrossRef] [PubMed]
63. Cardona, M. *Modulation spectroscopy. Solid State Phys. Supplement 11*; Academic Press: New York, NY, USA, 1969; ISBN 978-0-12-607771-1.
64. Pollak, F.H.; Shen, H. Photoreflectance characterization of semiconductors and semiconductor heterostructures. *J. Electron. Mater.* **1990**, *19*, 399–406. [CrossRef]
65. Chomette, A.; Deveaud, B.; Regreny, A.; Bastard, G. Observation of Carrier Localization in Intentionally Disordered Gaas/Gaalas Superlattices. *Phys. Rev. Lett.* **1986**, *57*, 1464–1467. [CrossRef]
66. Dal Negro, L. *Optics of Aperiodic Structures: Fundamentals and Device Applications*; Jenny Stanford Publishing: Singapore, 2013.
67. Barriuso, A.G.; Monzón, J.J.; Sánchez-Soto, L.L.; Felipe, A. Comparing omnidirectional reflection from periodic and quasiperiodic one-dimensional photonic crystals. *Opt. Express* **2005**, *13*, 3913–3920. [CrossRef]
68. Maciá, E. Exploiting quasiperiodic order in the design of optical devices. *Phys. Rev. B* **2001**, *63*, 205421. [CrossRef]
69. Maciá, E.; Domínguez-Adame, F.; Sánchez, A. Effects of the electronic structure on the dc conductance of Fibonacci superlattices. *Phys. Rev. B* **1994**, *49*, 9503–9510. [CrossRef] [PubMed]

70. Dal Negro, L.; Yi, J.H.; Nguyen, V.; Yi, Y.; Michel, J.; Kimerling, L.C. Spectrally enhanced light emission from aperiodic photonic structures. *Appl. Phys. Lett.* **2005**, *86*, 261905. [CrossRef]
71. Bhattacharya, R.N.; Shen, H.; Parayanthal, P.; Pollak, F.H.; Coutts, T.; Aharoni, H. Electroreflectance and photoreflectance study of the space-charge region in semiconductors: (In-Sn-O)/InP as a model system. *Phys. Rev. B* **1988**, *37*, 4044–4050. [CrossRef] [PubMed]